Magnetic Assisted Stastical Assembly

by

Diana I Cheng

Submitted to the Department of Electrical Engineering and Computer Science
in partial fulfillment of the requirements for the degree of

Masters of Engineering

at the

MASSACHUSETTS INSTITUTE OF TECHNOLOGY

September 2008

Author .....
Department of Electrical Engineering and Computer Science
August 22, 2008

Certified by....
Clifton Fonstad
Professor
Thesis Supervisor

Accepted by..
Arthur C. Smith
Chairman, Department Committee on Graduate Students

Magnetic Assisted Stastical Assembly

by

Diana I Cheng

Submitted to the Department of Electrical Engineering and Computer Science
on August 22, 2008, in partial fulfillment of the
requirements for the degree of
Masters of Engineering

Abstract

The objective of this thesis is to develop a process using magnetic forces to assemble micro-components into recesses on silicon based integrated circuits. Patterned SmCo magnetic thin films at the bottom of recesses are used to provide forces to orient, align and retain micro-devices on silicon. The overall objective is to obtain functionalities not readily available from silicon device structures alone. This thesis was done in the context of assembling optoelectronic devices, specifically integrating vertical cavity surface emitting lasers (VCSELs), edge-emitting lasers (EELs), and light emitting diodes(LEDs) onto commercially processed Si-CMOS circuits.

This method, magnetically assisted statistical assembly (MASA), incorporates past methods such as Fluidic Assisted Self-Assembly (FASA) and Recess Mounting with Monolithic Metalization (RM3). Specifcally, MASA addresses the main limitation to the FASA method by adding a magnetic layer as a restraint to keep assembled components correctly positioned in recesses until the time bonding may occur. Thus, all components may be permanently bonded into place simultaneously saving both time and money.

This thesis will present simulations using Ansoft's Maxwell 3d providing general behavioral intuition for the behavior of a device over a target magnetic substrate. These results include using a rectangle instead of a circular disc and making recess depths greater than 2μm to overcome gravitational forces when inverting the substrate. Patterns of SmCo magnetic material, based on results from the simulations, included 50x100μm recesses containing either a solid rectangle, thirty 5x10μm rectangular pads, eighteen 5x10μm rectangular pads or four 5x10μm rectangular pads. Patterns of SmCo material also were experimented with using 50x50 μm square recesses containing either a solid square or nine 5x5μm square pads.

Experiments with various rectangular patterns showed evidence that upside down devices do not retain as well as right side up devices. It was also seen that four 5x10μm rectangular pads did not have enough magnetic material to retain even right side up devices. Solid rectangular patterns were also determined to have too much magnetic material to align and orient the device without recesses. Once recesses were added to the experiments, the pattern with thirty 5x10μm rectangles proved to assemble

the most devices with an assembly ratio of 90%. However problems occurred with fabricating perfect device shapes and thus mis-shapened devices were counted in the assembly ratio. Results from experimenting with square patterns with recesses show a 88% assembly ratio with a solid square pattern. This may be due to the symmetry of the square devices and therefore has higher probability of assembly than that of the rectangular devices.

Thesis Supervisor: Clifton Fonstad
Title: Professor

Acknowledgments

First and foremost, I would like to thank Professor Fonstad for all the guidance and support he has put into this project, and for giving me the opportunity to work on an interesting and innovative thesis. His patience and resources were imperative to the completion of this thesis and without his help I'd still be lost today.

Furthermore, I would like to thank Dr. Joseph Rumpler for all his mentorship in all stages of this project. Especially for all the expert advice he gave me on development processes and past experiences. He served as a mentor to both me and the project. His previous work was both educational and essential to my work. I owe many thanks to Joe for all the dedication and hard work he put into helping me throughout this project.

I would also like to thank Kerry Cheung for his expertise in EML and for always letting me drop by with my infinite questions and helping me solve any random problem I was stumped on. He was an excellent source of information in the beginning stages of this thesis. I also owe a thanks to Kurt Broderick for all his help training me on machines and keeping me safe in EML, as well as Dennis Ward for all his expertise in mask making and hydelburg operation. They both took the extra time to help me through the glitches I had encountered in EML.

I would also like to thank Professor Zhan for supplying me with the simulation software needed to model and predict the behavior of the devices. The software helped me properly understand the design issues and trade offs in the later half of the thesis.

Lastly, I would like to thank my family and friends for supporting me throughout my life, during this project and through the many endeavors during my time here at M.I.T.

THIS PAGE INTENTIONALLY LEFT BLANK

Contents

THIS PAGE INTENTIONALLY LEFT BLANK

List of Figures

THIS PAGE INTENTIONALLY LEFT BLANK

List of Tables

THIS PAGE INTENTIONALLY LEFT BLANK

Chapter 1

Introduction

Hybrid assembly of small microscaled devices has long been a challenge. Precision machines have been developed to assemble conventional device chips and dies. However, these can be large and costly and more importantly, they are not useful for the next generation of smaller and thinner device dies now being integrated directly on IC chips. To automate the assembly of these die, fluidic self assembly (FSA) has been introduced [4], however current implementations of FSA have yet to be totally successful. Using Magnetic Assisted Stastical Assembly (MASA) can alleviate the problems in conventional FSA. MASA exploits magnetic forces to attract and align microscaled devices in recesses during fluidic self-assembly.

1.1 Motivations for MASA

The idea of MASA is motivated by trends toward integrating more and more functionality on a single IC chip. This in turn has motivated the trend of heterogeneous integration. It is no longer true that all devices are fabricated out of silicon. Vertical cavity surface emitting lasers (VCSELs) for instance, are fabricated from gallium arsenide or indium phosphide based heterostructures.[1] Hybrid assembly is required to integrate such devices with Si IC's because such heterostructures can not be grown directly on a Si substrate. The mixture of different materials causes further assembly complications including sturdy contact layers and reliable adhesion between device

and substrate.

In the present day, without an optimal micro-assembly processes, companies have resulted to packaging chips using bulky methods such as flip chip ball bonding. This widely used technique uses fully processed dies and bonds them face down using solder balls to create a firm contact. Unfortunately, this method greatly increases the size of the device constraining it to at least 1 mm^2 defeating the main benefit of scaling downwards [2]. In addition, this process requires very flat surfaces to mount on, but as heterogeneous devices such as the VCSEL are fabricated, these flat surfaces may require adding additional surface area. The cost of such packaging often outweighs the advantages of reducing the device size.[2]

The need for improved assembly techniques is the primary motivation for this research. As described in Section 1.2, the several existing methods have a wide range of problems. These problems are anticipated to be eliminated with the proposed method of MASA.

1.2 Current Integration Methods

Recently developed methods such as Pick and Place, Magnetic Field-Assisted Assembly, and Fluidic Self Assembly have shown improvements in successful bonding rates, alignment, and connectivity. However, each of these previous methods has its advantages and disadvantages which will be described below.

1.2.1 Microscale Pick and Place

A brute force method, Microscale Pick and Place, was developed at MIT in 2005. This method involves the use of a vacuum tube micropipette manually placed over the OptoPill (a VCSEL substitution used in assembly research). The pill is then suctioned to adhere to the beveled surface of the pipet, lifted, and then positioned over the desired VCSEL recess (or well in the substrate). After manual alignment, the suction is replaced by a positive pressure and the OptoPill is released into the recess. Figure 1-1 demonstrates a general schematic of this process.

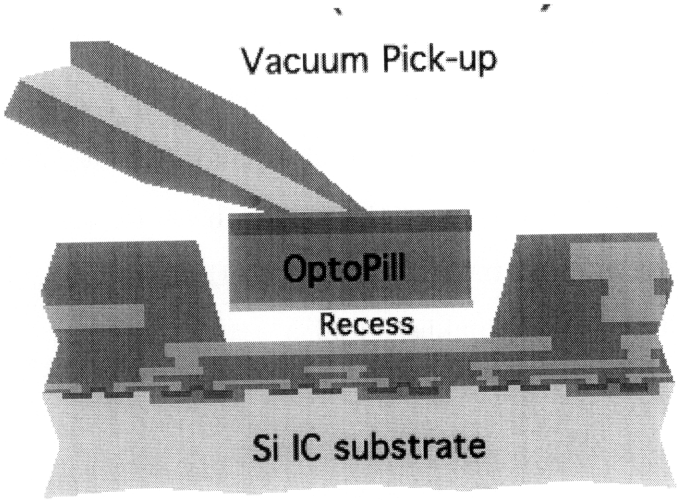

Figure 1-1: An overview schematic of the Microscaled Pick and Place process developed at MIT in 2005.

The need to manually align each individual OptoPill is very inefficient and unattractive to use for mass production. Furthermore, each pill must be manually aligned and complications often arise during the releasing of the pill into the recess. Researchers report that pills were often blown far away from the target recess by the vacuum tube. Pills also can become charged and attract to the pipet, thus complicating the release process. Environmental factors such as airflow and humidity of the room also significantly decreases the success rate of this process [2].

However, because everything is preformed manually, this method holds the possibility of good accuracy. Once assembled properly, the device is very likely to be oriented and aligned inside the recess correctly. This could prove to be a big advantage for devices with odd geometric shapes with a front and back face. Past research has shown this technique has a 54% success rate in a labratory setting[2].

1.2.2 Magnetic Field-Assisted Assembly

In 2004, Magnetic Field-Assisted Assembly was hypothesized as a new approach to nanoscaled semiconductor devices assembled onto silicon[3]. This technique involves running a strong magnet on the underside of a substrate wafer while at the same time rolling a feeding tape of devices over the substrate. Figure 1-2 shows a general

schematic of the system. The idea was for the devices to roll off the feed tape onto the substrate and stick due to the magnetic forces. The main advantage to this method was that it required no liquids leading to clean and dry environments. However it is very dependent on the precision of the guide wheels for the feed tape. Unfortunately this method was never tested, just hypothesized as a theory and thus has no experimental results have been published [3].

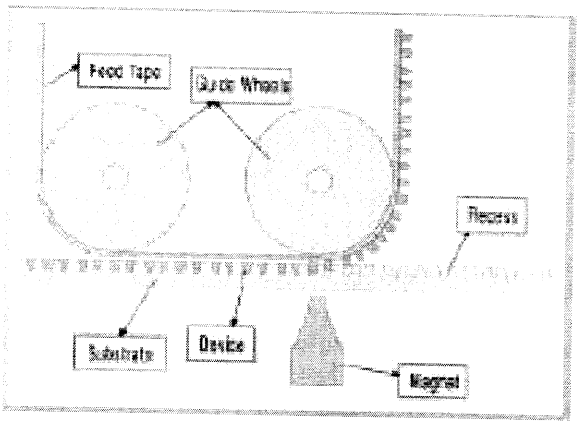

Figure 1-2: A schematic of a hypothesized approach to nanoscaled assembly called magnetic Field-Assisted Assembly.

1.2.3 Fluidic Self Assembly

Fluidic Self Assembly is a technique that involves suspending devices in an methonal solution and then running the solution over the substrate at an designated angle as shown in Figure 1-3. At the proper flow rate and designated angle, the van der Waals force are said to be enough to hold down the devices into the wells [4].

The results of this technique proved to be quite successful. With circular devices, there was a 100% fill rate. [1] It was initially observed that devices would stick to the sides of the wells and thus would cause obstructions to the nearby wells. To improve the system, a sonic vibration was added to the system to dislodge these obstructions.

This process has a few advantages over the pick and place method as it is more

[1]Fill rates were calculated based on satisfying the following rate equation $\frac{dn}{dt} = p\lambda(1-n)$ where n is the fill ratio.

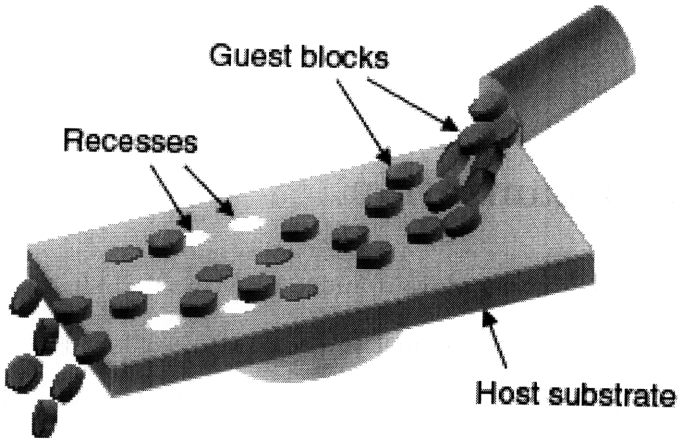

Figure 1-3: An overview of the fluidic self assembly process (FASA). Note devices are assembled regardless of front or back face

conducive to large scale manufacturing. The process is quite automated and requires minimal manual supervision. The setup cost is also quite minimal as only a flat surface and a flowing valve mechanism is necessary. Devices are rarely wasted in this process as the solution may be collected at the bottom and recycled back through the top. Furthermore, this technique allows for easy trials until the substrate is completely assembled.

A drawback of the system is the lack of ability to orient the devices in the recesses. The orientation of the devices is left up to chance as they wash over the substrate. A device can be easily assembled upside down without any obstacles to distinguish this mistake. Furthermore, the biggest disadvantage of the system is the tendency for of devices to fall out of the recesses almost as fast as they fall in. It was shown that the devices were not securely held into place and would fall out of place before bonding could occur. While the success rate of this process is 100% for larger devices (150μm on one side), it has limited success for smaller devices [4]. Furthermore, geometric shape proved to have an contribution to the success rates as well. This technique was shown only to be effective for circular shaped devices whereas square shapes saturated at 40% fill rates.

None of these past techniques address the orientation and alignment of devices in silicon. It is imperative for certain devices such as wave guides, to be aligned in the

silicon. MASA addresses orientation as well as alignment issues during assembly of such devices.

1.3 Thesis Organization

Past research has led to further development of MASA. The next few chapters describe the work accomplished in the last few years to progress this technology. Chapter Two details the simulations performed using Ansoft Maxwell 3D software. These answer preliminary questions on the behavior of the devices and the hard magnetic substrates, included optimizing sizes and material thicknesses. General conclusions on the behavior of the devices are outlined here. Chapter Three continues on to describing the materials needed for the lab experiments and what is involved with fabricating these substrates. The experimental setup is described as well as the design considerations that went into determining flow rate, angle of flow and container setup. Magnetic loops are also shown here to illustrate the hard SmCo remenant magnetization. Recess design and process is described as well as the design and process of patterning magnetic SmCo substrates. Chapter Four presents the experimental results and conclusions. The data collected from running experiments without recesses, rectangular shapes with recesses, and square shapes with recesses, is both described and plotted here. In this chapter, problems encountered during the experiments is further described and analyzed. Results and conclusions are summarized in this chapter also. Lastly, Chapter Five suggests future work and improvements to progress the technology of MASA.

Chapter 2

Theory and Simulations of MASA

2.1 Theory of MASA

Magnetically Assisted Statistical Assembly (MASA) combines magnetic retention and orientation with Fluidic Self Assembly (FSA). The concept involves patterning a ferromagnetic thin film on hard magnetic material in Figure 2-1, at the bottom of a recess. Then recesses are build above the substrate. The pattern used is designed to both hold the devices in their recesses and to orient the device correctly within the recess. Afterward, the substrate is processed through FSA which allows the devices to float over the substrate. The soft magnetic material on the devices is attracted by the magnetic pattern and with a properly designed pattern, an attraction much greater then Van der Waals forces will orient and hold the properly assembled devices at the bottom of the recess until they can be bonded permanently in place. This extra force will help segregate properly assembled devices from devices not in the target position on the substrate. This method is a member of the RM^3 family of techniques.

2.1.1 Motivations for RM^3

Recess mounting with monolithic metalization (RM^3) is an integration tactic proposed as a means to integrate heterogeneous materials on Si substrates. This technique involves either growing devices into recesses or growing devices separately and then

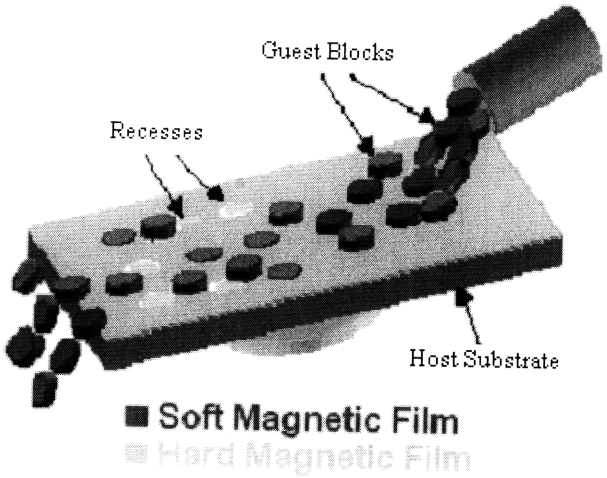

Figure 2-1: An overview of the magnetic assisted statistical assembly process (MASA). Notice devices are only assembled when front face is pointing upwards.

later assembling them into position in recesses. Figure 2-2 shows the steps of the process. Advantages of assembling devices into recesses include planer surfaces for contact layers as well as wafers being 3-d ready. Also, in MASA applications, recesses are used as guides to orient the devices in position until bonding.

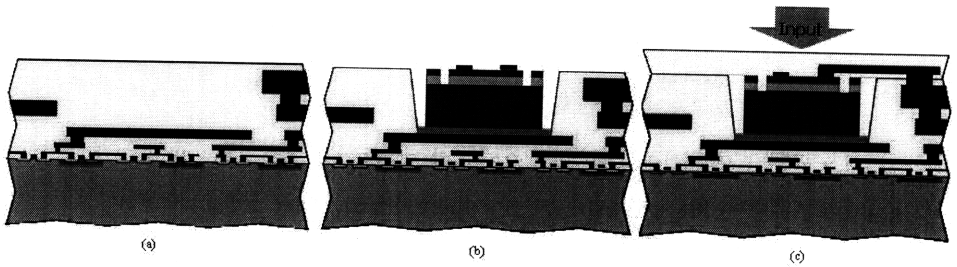

Figure 2-2: An overview of the steps for an RM^3 type procedure involving recess assembly and bonding. In the sequence, (a) shows an IC chip before assembly, (b) shows an device properly assembled into the recess on the IC substrate, and (c) shows direct pin contacts between the IC chip and the device completing the RM^3 procedure.

2.1.2 Advantages of MASA

Many of the advantages of other fluidic assembly processes are also inherent in MASA processes. First, MASA does not restrict or compromise the processing of the high quality devices being integrated leading to greater flexibility in the application of the process. Secondly, MASA allows for device yield testing prior to integration as each

device is a stand-alone device before being assembled. Third, as MASA is part of RM^3 processes, a planar topology is possible for high volume manufacture assembly.

MASA also takes advantage of metal to metal bonding, similar to flip chip bonding techniques. MASA targets large scaled production so vast quantities of devices can be integrated simultaneously. Furthermore, MASA enables efficient use of semiconductor material as devices can be patterned and processed in close packet arrays independent of the final pattern and/or density in which they are integrated. Mainly, because MASA involves integrating independent devices, where as previous technology requires the assembly of arrays of devices, MASA involves a great deal more flexibility than previous processes.

2.2 Simulations Using Ansoft 3M Software

2.2.1 Prior Modeling

Prior preliminary calculations have been preformed using MatLab software to model the attractive forces between device and magnetic substrate. These calculations model a periodic array of perpendicular anisotropy hard magnetic stripes with a layer of soft magnetic film. The results of the modeling support the idea that the strength of the attractive forces can be engineered and tailored through the design of the hard magnetic films (SmCo patterns).

This may be seen in Figure 2-3, showing preliminary evidence that the magnetic strength falls in a predictable behavior [5]. [1] The log-linear graph shows linear variation of the log of the attractive force and thus we expect to see exponential fall-off of the force with the separation of the device from the magnetic patterns.

[1] the first order magnetic force density is modeled by the expression

$$F_Z = -\frac{\mu_0 M_r^2}{\pi^2}\left[e^{-2k_y g}\right]\left[1-e^{-k_y d}\right]^2\left[\frac{\left(e^{2k_y t}-1\right)\left(\mu_s^2-1\right)}{e^{2k_y t}(\mu_s+1)^2-(\mu_s-1)^2}\right]$$

where M_r is the hard magnetic film remanent magnetization $k_y = \frac{2\pi}{L_y}$, and L_y is the pattern period.

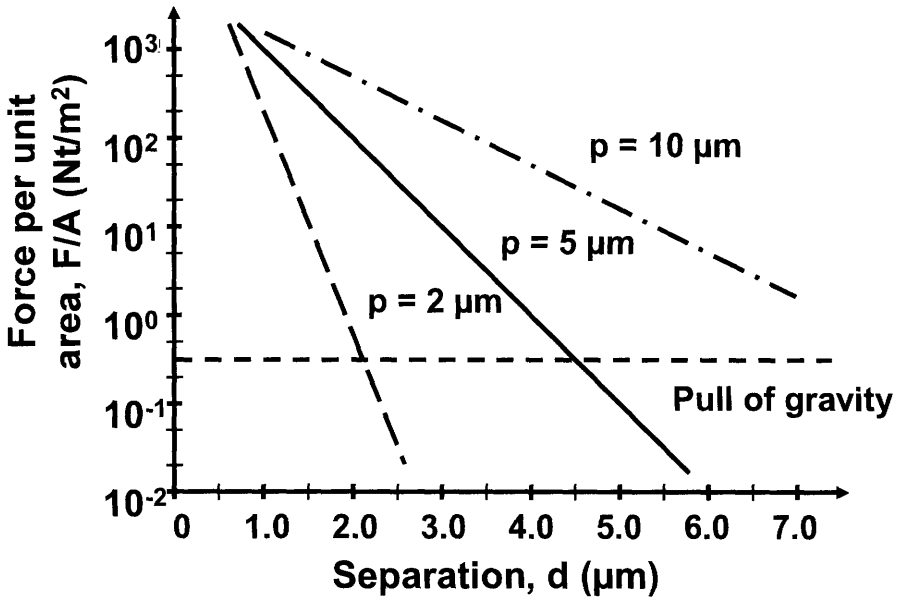

Figure 2-3: Preliminary Matlab simulations, using bars of hard magnetic material in the x direction. This plot shows that the attractive magnetic force between the device and the magnetic material increases exponentially with decreasing separation, and that the extent of the attraction depends on the period of the hard magnetic material patterns.

2.2.2 Setting up Ansoft 3D modeling

To further predict behaviors of different hard magnetic film patterns, Ansoft software was used. This software package included models of SmCo magnetic characteristics as well as nickel metal used. SmCo material is the hard magnetic material patterned on the target substrate and the nickel is the soft magnetic material layered on the devices being assembled.

The modeled nickel used in the simulation was 0.5μm thick. The modeled Samarium Cobalt used was SmCo24, 0.5 μm thick. The polarity was set constant in the x direction with global coordinates to ensure consistency. An outer boundary setting a parameter around the simulation was set to be twice the size of the simulated field. This outer boundary was chosen large enough to encapsulate predominate magnetic field strengths while keeping the software runtime from becoming excessive. The area was filled with vacuum parameters, consistent with the non-magnetic nature of aqueous elements of the experiment. Other parameters such as boundaries, excita-

tions, hash operations and optimetrics were set to null as our hard magnetic material behaved like a permanent magnet.

Accuracy of the program is measured in convergence and energy. Only energy errors of less then 0.03% were accepted as accurate and repeatable conclusions. General error was required to be less than 0.01 and a minimum of two convergence passes had to be satisfied. All these constraints were required to create a repeatable simulation to the hundredth degree. Furthermore, high accuracy tetpoints of up to 100 were set to ensure all field lines were captured as seen in Figure 2-4. More tetpoints (or points of measured field strenth) equated to more accuracy of the magnetic fields (or B fields).

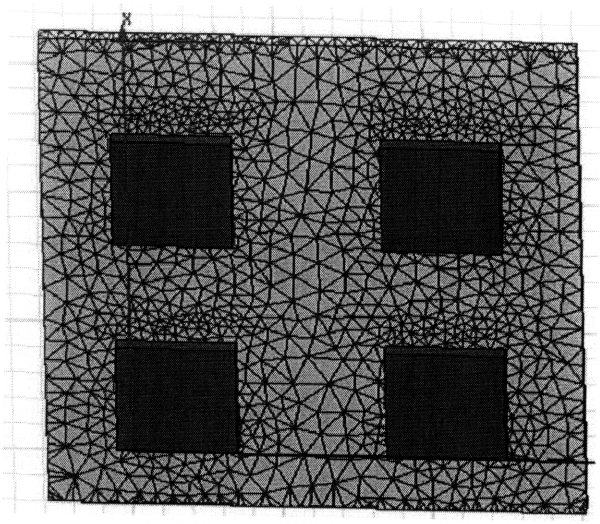

Figure 2-4: Parameters entered into the Ansoft Maxwell 3D simulation program specifying an mesh, where each intercept, called a Tet point, is a force calculation point. The more dense the mesh, the more accurate the force calculation.

2.2.3 Retaining Forces

The purpose of the simulations is to model the magnetic field effect on the device, gaining intuition for the amount of force necessary to overcome the gravitational force of an inverted substrate. Gaining intuition for the behavior of force between magnetic material and device will dictate designs to later fabricate and experiment with.

Squares versus Discs

Initially, a geometric shape for the devices had to be decided upon. As it seemed that a device could be made into any shape, a geometric figure that gave the most information about assembly movement would be desired for the experiments.

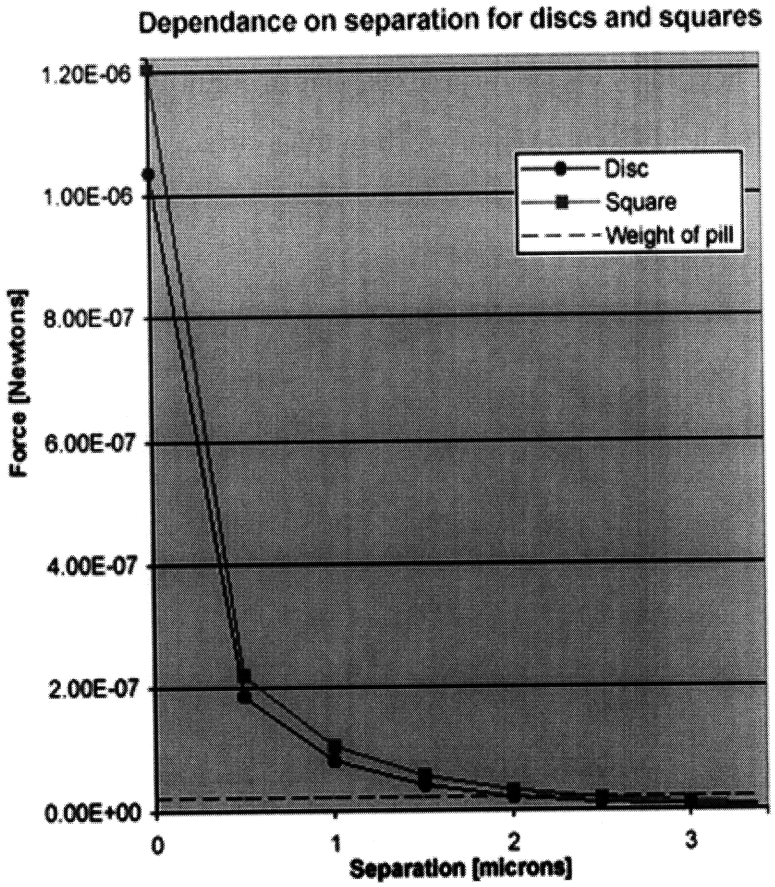

Figure 2-5: The result from plotting attractive force versus separation displacement in the z direction for both square and disc dimensions. Disc dimensions were 5μm in diameter and square dimensions were 5 by 5μm.

Simulations were conducted to choose between experimenting with disc or square devices. Disc devices would be 50μm in diameter and 5μm in height as most of the devices available were of that dimension. The square device simulated was 50x50μm and also 5μm in height. These dimensions will resemble the actual device dimensions used in experiments in laboratory settings providing more accurate intuition for ex-

periments later on. It can be seen in Figure 2-5, the attractive force behavior of both geometric shapes is very similar and thus either shape would work. However, it was thought that the disc shape would provide less information on being able to align and orient the devices into the recesses and thus it was decided to use a rectangular device. Further simulations were applied to squares as the processing power for an accurate rectangle simulation was larger than the hardware available.

Force Relative to Device Weight

The ultimate advantage of MASA is the added retention force during FASA. This retention force during assembly increases the probability devices stay assembled during the entire process. To simulate this probability, gravitational force of the device is calculated. Ideally, the substrate could be inverted and the properly oriented devices would stay assembled until bonding, allowing for better success rates and more time efficient processes.

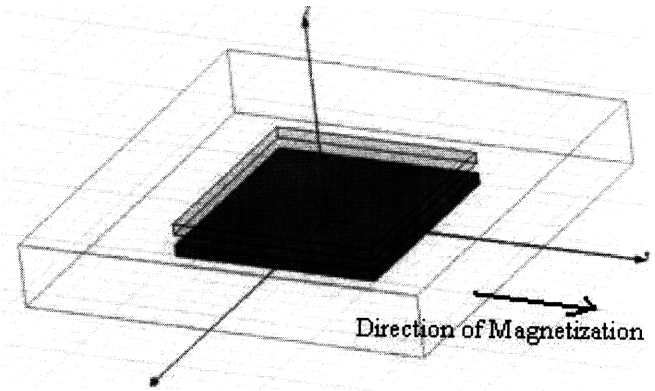

Figure 2-6: The simulation setup for a 5x5x0.25μm Ni plate, varying separation distances from a 5x5x0.25μm SmCo magnetic plate in the z direction. The Ni plate is the transparent plate on top of the dark shaded SmCo magnetic plate. The results are shown in Figure 2-7 and Figure 2-8.

The purpose of the next simulation set is to determined the minimum retentive force needed to overcome the gravitational force of the 5x5μm Ni device while varying separation distances between the 5x5μm SmCo square. This setup can be seen in Figure 2-6. The devices used in later experiments were estimated to cause approximately 1.2x10^{-9} newtons of gravitational force. This calculation is as follows,

weight of a 5x5x0.25μm Ni square is calculated as
force= $(5x5x0.25)\left(\frac{1cm}{10^4\mu m}\right)^3\left(\frac{8.89g}{cm^3}\right)\left(\frac{1kg}{1000g}\right)9.8 \approx 5.44x10^{13}$N added to
GaAs force using a 5x5x4.75μm device has a force $\approx 6.19x10^{-12}$N

Practical experiments performed later have Ni dimensions of 50x50x0.25μm resulting in a force $\approx 1.09x10^{-9}$N added to
a force $\approx 1.24x10^{-10}$N for a GaAs layer using 50x50x4.75μms.

Referring to Figure 2-7, it can be seen that any separation less than 2μm would create enough force to keep the device from falling out of an inverted substrate. This implies the contact layers of gold and gallium arsenide must be thinner than the minimum separation distance of approximately 2 microns.

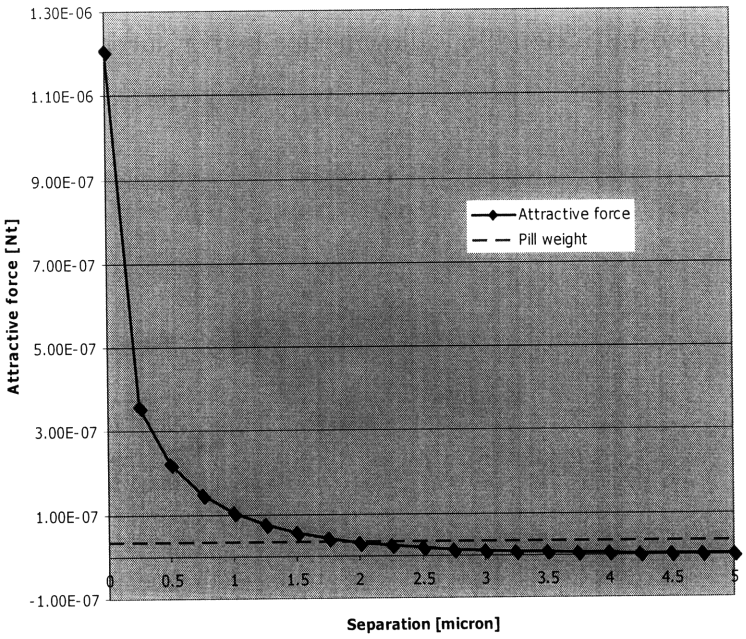

Figure 2-7: The result of plotting attractive force versus separation distances in the z direction between a 5x5x0.25μm Ni plate and a 5x5x0.25μm SmCo magnetic plate, as illustrated in Figure 2-6. Pill weight is calculated for a 5x5x5 device

The variation of the attractive forces with distance is either quadratic or exponential. As seen in Figure 2-8 a linear-logarithmic plot shows linear correlation between attractive force and separation distance in the z direction. This indicates that the space between the device and the magnetic material can rapidly affect the success of

the assembly process.

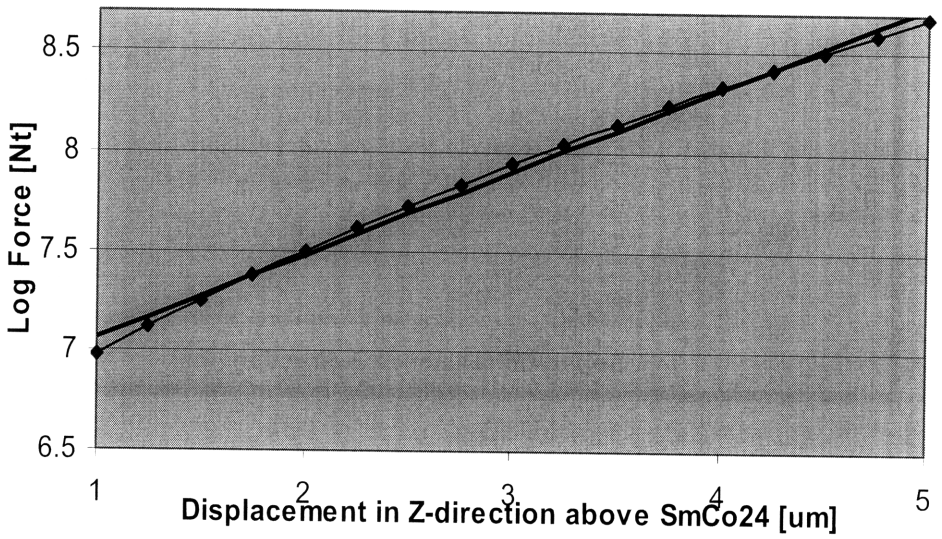

Figure 2-8: The result of plotting attractive force versus separation distances in the z direction between a 5x5x0.25μm Ni plate and a 5x5x0.25μm SmCo magnetic plate, on a logarithmic scale. Setup can be seen in Figure 2-6.

Variation with Square Sizes

Once rectangles and squares were decided upon, the sizes of both device and magnetic material dimensions were both modeled. Both SmCo and Ni squares were scaled to the same dimension as in Figure 2-6. With squares, the simulation was rather uniform, meaning an increase in one edge required an increase in the other edge. Knowing that the target patterns, to be experimented with later, would be around 5μm in length and width, a 5μm, 3μm, and 1μm set was simulated. Decreasing both Ni and SmCo sizes simultaneously shows consistency with previous MatLab modeling that the fall off is faster for the finer period devices. The results are shown in Figure 2-9.

The results shown in Figure 2-9 indicate that smaller squares lead to a much faster fall-off rate for retentive forces. With a faster fall off rate, precise engineering of the magnetic material is needed as the system becomes more sensitive to variation causing fluctuating assembly results. With a slower fall off rate, the system is more suitable to account for experimental variation. However, a slow fall off rate may cause too much attractive force causing inverted devices to miss assemble. A balance needs

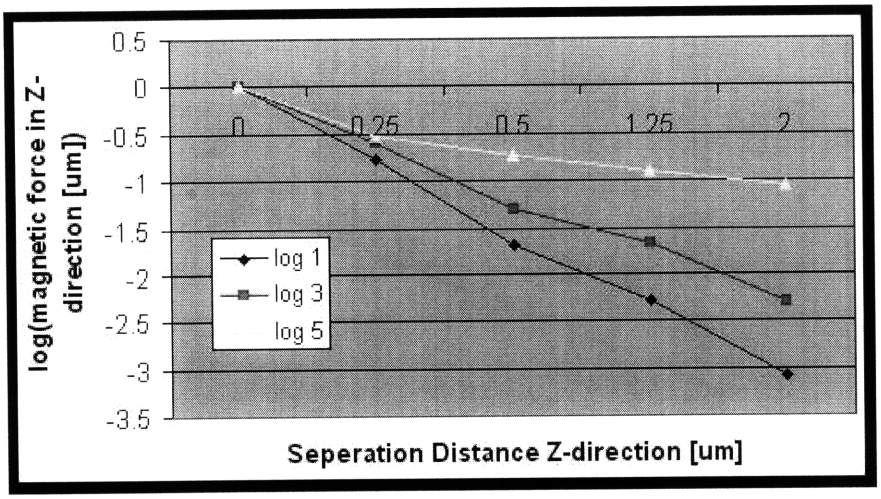

Figure 2-9: The result of a semi-log plot varying Ni and SmCo dimensions, keeping both equal in shape. The graph plots force versus seperation in the Z-direction.

to be achieved such that the fall off rate satisfies both considerations. The fall off rate for the smaller squares were felt to be too rapid for experimental consistency as well as from fabrication stand points, larger squares were better. Therefore the 5μm design was chosen.

Optimizing Device Size vs. SmCo Squares

The next question involves finding the optimal device size relative to magnetic material dimensions. In the setup, the size of a nickel plate is varied over a constant 5x5x0.25μm SmCo square, as illustrated in Figure 2-10. Varying the dimensions of the nickel plate will find the optimal device size for a given hard magnetic pattern. The thickness of the plates were both kept at a constant 0.25μm but varied the surface area. Also, the attractive force between the nickel and the magnetic material was measured at a fixed separation distance of 0.5μm.

Attractive force simulations were done with Ni square sizes of 4x4,5x5,6x6,7x7 and 8x8μm. Varying the surface area of the Ni plate resulted in the variation shown in Figure 2-11. There is a rapid increase in the attractive forces as the size of the Ni plate increases, however, if the size of the Ni exceeds that of the SmCo, than the force actually decreases although much more gradually. In Figure 2-11 it could be seen that the force decreases when the Ni plate exceeds 6x6μm and peaks at dimensions

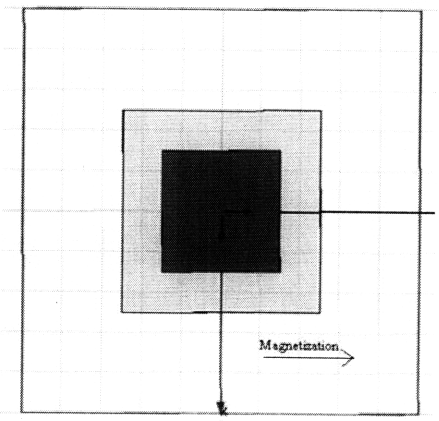

Figure 2-10: The simulation setup to test optimum device size, given a constant 5x5x0.25μm SmCo square. All separation distances were kept at 0.5μm and all plate thicknesses were constant at 0.25μm. Shown, is the simulation with a 5x5x0.25μm SmCo square with a transparent 7x7x0.25μm Ni square on top. Results shown in Figure 2-11

of 5x5μm. It is speculated that this behavior is a result of the fringing magnetic field lines having decreased effect on the Ni plate at greater distances. The figure indicates that a Ni square approximately the same size as the SmCo magnetic material is the optimal pill size in order to eliminate unnecessary material costs while still capturing sufficient amounts of retentive force.

Additive Squares

Ultimately, sparse patterns of magnetic squares may provide a way to design and engineer the forces to align devices into recesses. Different magnetic patterns will provide different amounts of force and thus different alignment and orientation forces. Patterning the material will give user flexibility in controlling the assembly process.

To do this, a setup was created testing the effects of adding an 5x5x0.25μm SmCo square each with 5μm separations. Individually, they were added in a row along the y direction, each time centering the entire pattern. A 55x5x0.25μm Ni structure was used to simulate a device, consistently placed 0.5μm above the substrate, keeping the long edge along the y axis. Forcing the Ni plate to be large enough, while adding SmCo squares beneath, captures sufficient fringing magnetic field lines to keep the

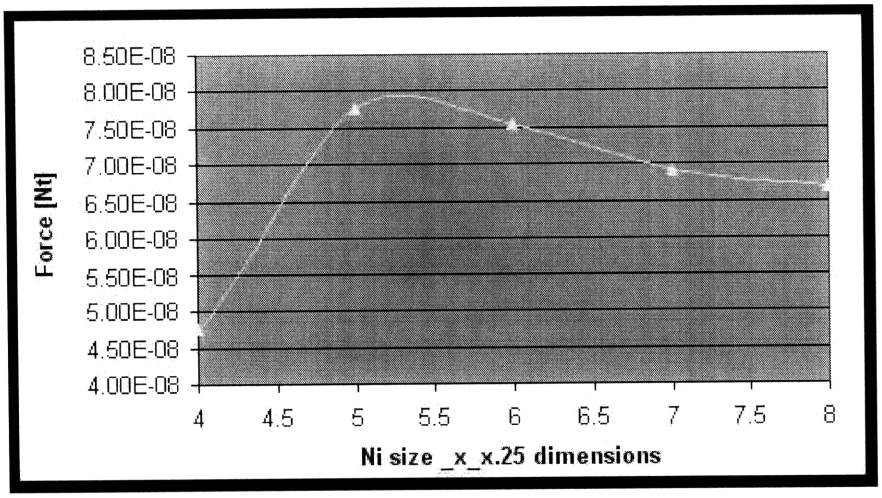

Figure 2-11: The result of plotting attractive force versus different Ni square dimensions while keeping the SmCo square constant at 5x5x0.25μm, refer to Figure 2-10. The optimum Ni plate relative to SmCo dimensions is determined to be approximately the same size as the underlaying SmCo reference frame. All separation distances were kept at 0.5μm and both plate thicknesses were kept at 0.25μm.

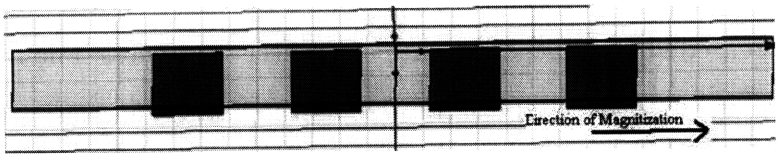

Figure 2-12: A simulation setup showing a maximum of four 5x5x0.25μm SmCo square plates underneath a 55x5x0.25 μm plate of Ni. Attractive force calculations are measured in the vertical(z) direction. Results as shown in Figure 2-13.

calculations consistent. Refer to Figure 2-12 for a graphical image of the simulation setup. The polarity of the SmCo was set in the x direction, thus same amounts of magnetic field are captured between each run. By limiting the fringing field effect for all SmCo squares in the y direction, the variance of the fringe field due to the increasing number of SmCo squares was minimized.

Adding one SmCo square at a time, for up to four squares, the results can be seen in Figure 2-13 below. The attractive force on the Ni plate increases linearly with the number of squares. As seen in the figure, each SmCo square is separated by a 5μm space which does not seems to effect the force calculations, as the Ni plate is long enough to capture equal amounts of fringing fields. The linearity shown supports the concept that instead of one solid block of SmCo, patterns of smaller blocks can be

designed to have the desired total retentive forces. Such patterns of squares may also be used to align pills to an underlaying reference frame.

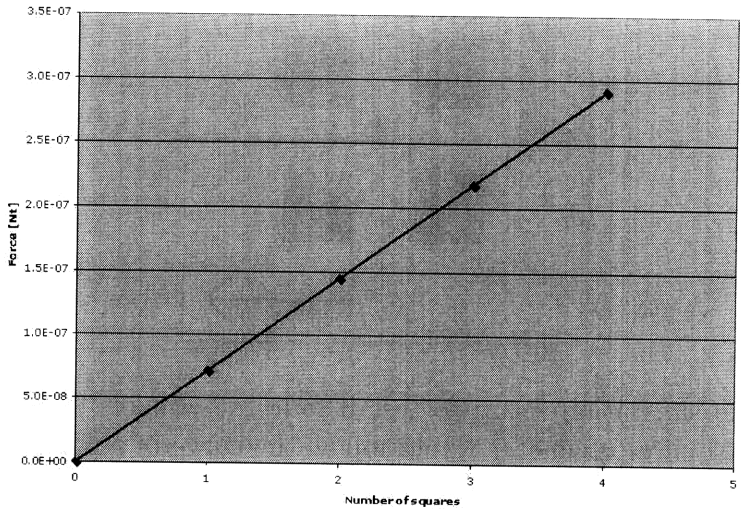

Figure 2-13: The result of plotting attractive forces between a 55x5x0.25 μm Ni plate and SmCo material versus the number of 5x5x0.25μm SmCo squares added. The structure is illustrated in Figure 2-12.

Grids

The desired rate of fall off for the attractive field occurs for SmCo squares on the order of 5μm per side, so for larger devices it seems to be necessary to use an array of these smaller SmCo squares. Thus grids of SmCo squares were modeled to verify that the predicted behavior of a single SmCo square is not interfered by the grid design. Specifically, the simulation is meant to compare four 1x1x0.5 squares of SmCo in the four corners of a 3x3 square parameter with a 3x3 solid square piece of SmCo. The setup may be seen in Figure 2-14. Following, the results of the grids can be seen in Figure 2-15 on page 40. Indeed the behavior shows very similar results. The only difference seen is the solid square has a slight increase in attractive forces which is accounted for by the grid formation lacking extra magnetic material between each of the smaller squares in the corners. It was also seen in the simulations that smaller dimensioned grids had faster fall off rates than larger dimensioned grids. Therefore

the behavior of grid SmCo is similar to the solid SmCo squares simulated before.

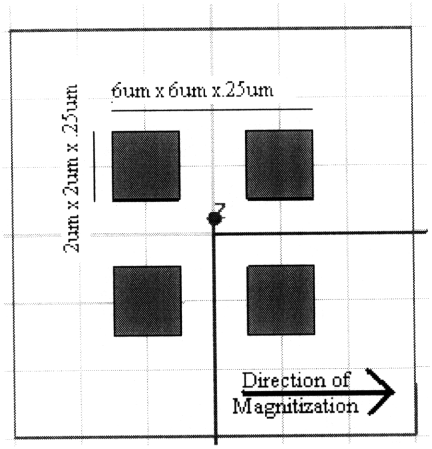

Figure 2-14: The simulation setup to test if four 2x2 squares of SmCo in the four corners of a 6x6 square parameter would follow the curve of a 6x6 solid square piece of SmCo. Refer to Figure 2-15 below.

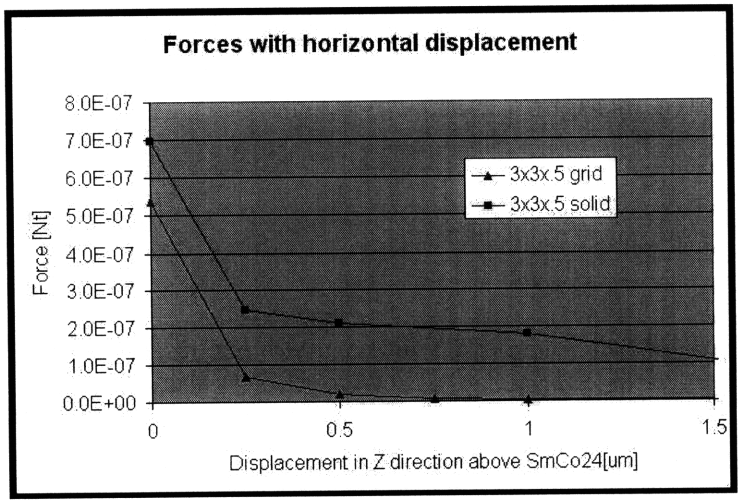

Figure 2-15: The result of plotting attractive forces for a grid of four 3x3x0.5 creating a 6x6 parameter and a solid 6x6x0.5 square piece. These forces are plotted versus displacement in the z direction. Refer to Figure 2-14 for simulation setup.

2.2.4 Aligning Forces

During FASA, devices are floated over the substrate with magnetic material, pulling the devices down from suspension into recesses. This attraction is gradual, incrementally pulling the device into the center of the recess. Thus further modeling of

misaligned devices at different distances and separations is needed to predict these incremental behaviors.

Displacements in X and Y Directions

The setup for the simulation involves taking 5x5x0.25μm squares of Ni and shifting it over a 5x5x0.25μm square of SmCo as illustrated in Figure 2-16. By intuition, shifting the Ni square in the x direction would cause a local maximum as the SmCo square is polarized in the y direction. Shifting the Ni square in the y direction would cause gradual decrease in attractive forces. This would be due to the increasing distance between the magnetic material and the device.

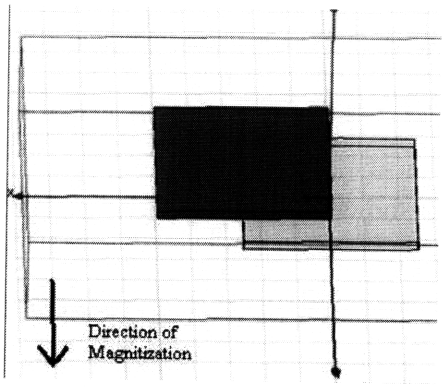

Figure 2-16: The simulation setup showing a 5x5x0.25μm Ni square and shifting it over a 5x5x0.25μm SmCo square in the x direction, measuring attractive forces in the z direction. Refer to Figure 2-17 for simulation results.

Based on the Figure 2-17 below, it can be seen that the attractive forces are predicted to be greater than the pill weight at distances greater than 0.25μm from the center. This restraint is only valid for the x direction as the y curve does not cross below pill weight until after 3.5μm misalignment. As the distances decrease, the attractive forces between the Ni square and the SmCo square decrease. This indicates that if the pills can move readily, then precise alignment is probable.

To enforce the idea that grids would produce similar characteristics, another set of simulations was applied to a grid of SmCo squares like that in Figure 2-18. This is to ensure that the grid formation would react to x and y device misalignments similarly

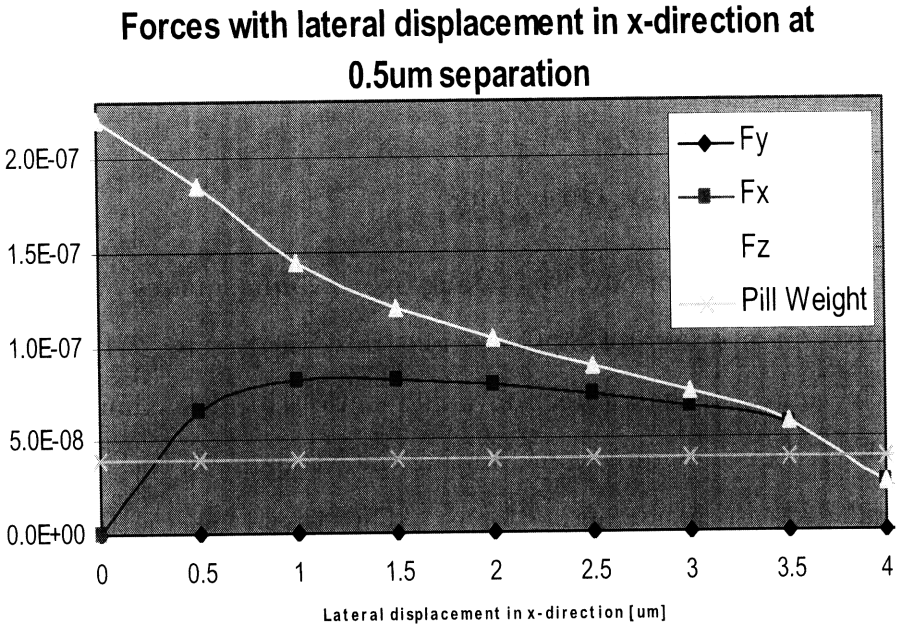

Figure 2-17: The result of plotting attractive force in the z direction versus the amount of displacement, between a 5x5x0.25μm Ni square over a 5x5x0.25μm SmCo square, in the x direction. Refer to Figure 2-16.

as before. These results are shown in Figure 2-19 on page 2-19 which illustrate a potential problem.

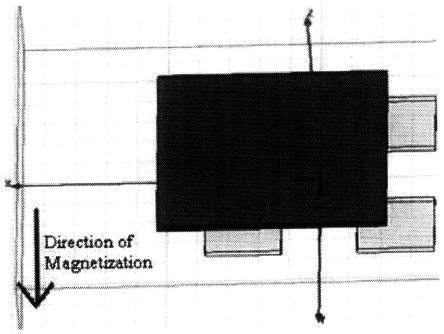

Figure 2-18: The simulation setup of a 5x5x0.5μm Ni square being displaced in the x direction over a grid of 2x2x0.5μm SmCo squares. Shown is a displacement of 1μm in positive x direction, refer to 2-19 for simulation results.

Local minimums and local maximums are observed in the graph of force vs. lateral distance in the x direction. This indicates that at a certain distance, there might be more attractive force than desired as this attractive force might lead to misalignment. If not designed exactly on the border, this local maximum can restrict the device from sliding readily into the proper place. This shows that on a grid pattern,

misalignments are more probable. Therefore recesses were chosen as they reduce lateral misalignment.

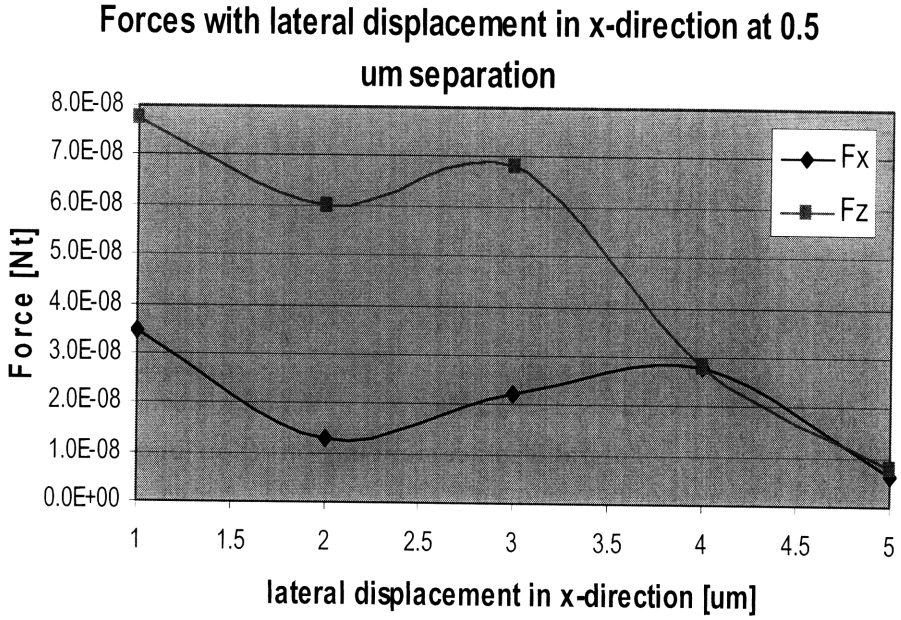

Figure 2-19: The result of plotting attractive force in the z direction versus the amount of displacement, between a 5x5x0.5μm Ni square over a grid of 2x2x0.5μm SmCo squares, in the x direction. Refer to 2-18 for simulation setup.

The y direction misalignment was also modeled and graphed in Figure 2-20. This does not indicate any possible problems like the x direction. The forces for the y direction displacement are significantly smaller in magnitude. This indicates that flowing devices along the y axis would have less dramatic effect than flowing devices along the x axis. It was observed that there is a greater attractive forces along the direction of polarization.

Rotational Alignment

During FASA, the devices can be suspended in any orientation imaginable. This could result in the need for rotational manipulation from the SmCo pattern to fit the devices into the recesses.

To simulate this, rectangles of 5x10x0.25μm Ni plates were rotated above 5x10x0.25μm SmCo plates. The force simulations were done as the Ni rectangle was rotated at various angles around the central axis. Then restoring forces can be measured in a form

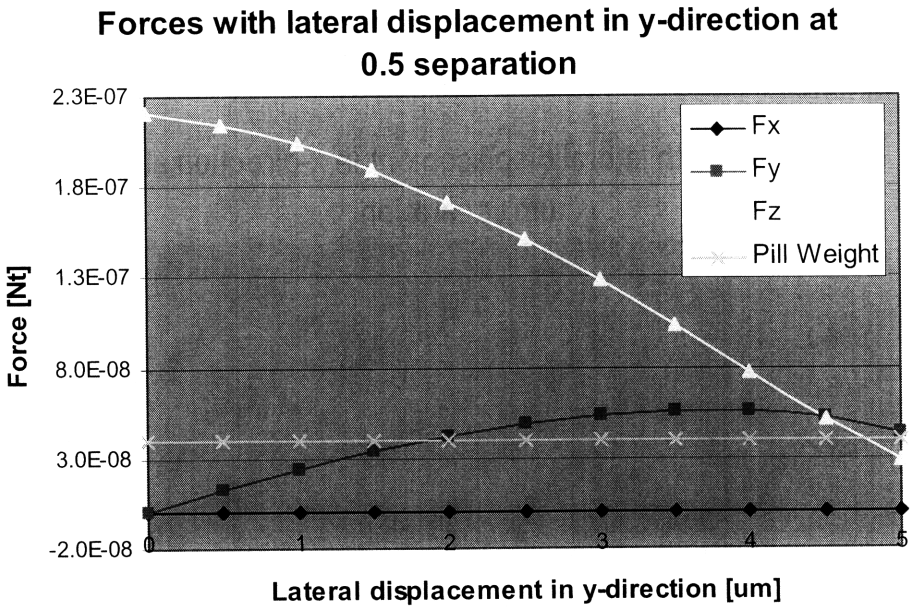

Figure 2-20: The result of plotting attractive force in the z direction versus the amount of displacement, between a 5x5x0.25μm Ni square over a 5x5x0.25μm SmCo square, in the y direction.

of torque as shown in Figure 2-21. The shape of the curve indicates that there is a maximum torque at approximately 45 and 135 degrees thus indicating a maximum restoring force at those angles. Also, a local minimum of torque occurs around 90 degrees. This could cause a problem as it indicates that devices rotated 90 degrees with respect to the recess will feel no restoring forces. However, assuming the recesses are thick enough, there should be sufficient distance between the SmCo and the device that the device will not be held and will be free to move into a recess. Once in a recess it will be well within 45^o of its proper position. Thus, with proper design, a rotational restoring force will align the device into the recess during assembly.

2.2.5 Layer Structure

The structure of the assembled circuit will be composed of gallium arsenide (GaAs), samarium colbolt (SmCo), nickel (Ni) and gold (Au) layers. This profile of metal, magnetic, and organic materials may not only effect the separation distances, but also the amount of attractive force felt by the device. The thickness of the nickel and SmCo layers should affect the magnitude of forces felt. Modeling of these layers show the

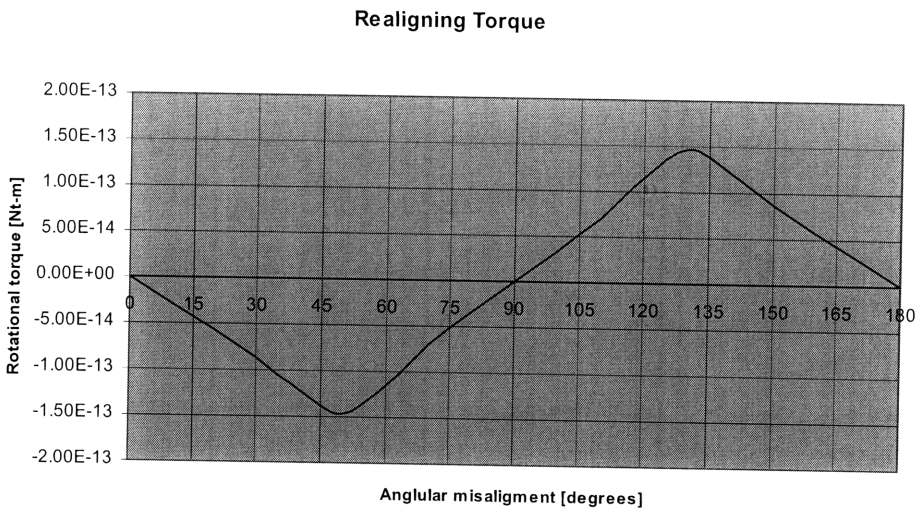

Figure 2-21: The result of plotting rotational torque versus angular misalignment of a 5x10x0.25μm Ni rectangle rotated 0.5μm above a 5x10x0.25μm SmCo rectangle.

exact effect of increasing Ni, SmCo and the other layers including the non-magnetic metals and organic material layers.

Optimum Magnetic Layer Thickness

By designing for the optimum magnetic layer thickness, excessive material costs could be avoided. The thicker the SmCo layer, the more costly fabrication becomes. Also variations in the fabrication process makes thinner layers more desirable.

As seen in Figure 2-22, 0.1, 0.25 and 0.5 μm thick Ni plates are paired with combinations of 0.1, 0.25, and 0.5 thick SmCo plates. These are then plotted against the magnitude of attractive forces between the Ni and the SmCo plate. The results indicate that varying the nickel thickness does not affect the attractive forces between the device and the magnetic layer. However, results do indicate that varying the SmCo thickness will drastically affect the magnitude of force. Thus it is inferred that there are no restrictions on the design of the contact layers on the device as the Ni thickness has minimal bearing on the assembly behavior. However the thickness of the SmCo must be controlled carefully.

For the pill weight previously calculated, a necessary volume of SmCo material is calculated based on the distance away from the SmCo pads as seen in Table 2.1.

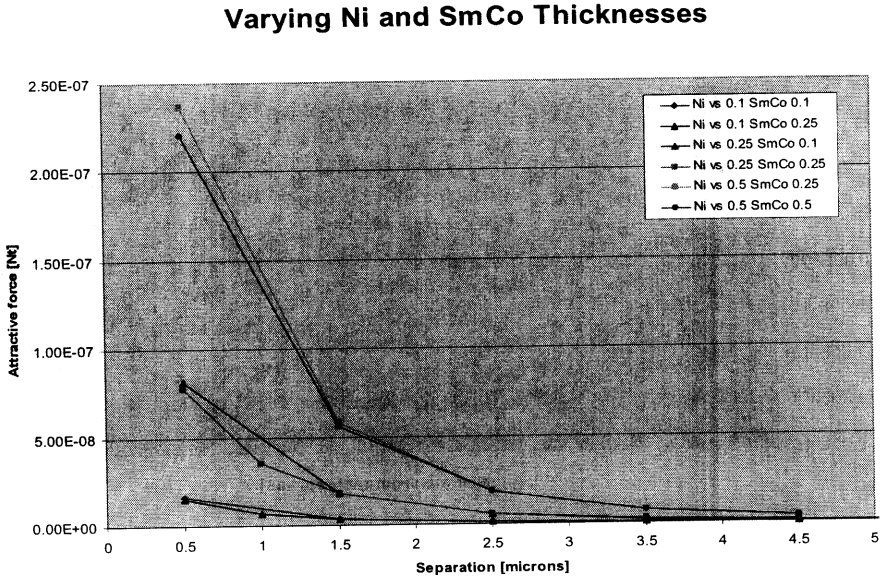

Figure 2-22: The result of plotting attractive force versus varying separation distances in the z direction for various combinations of Ni and SmCo thicknesses

These calculations are also translated into the number of 5 by 10 μm rectangular SmCo pads.

Table 2.1: Table of separation distances showing the necessary volume of SmCo material needed to constrain the device in an inverted substrate. The third column translates the volume of magnetic material into number of 5x10x0.25μm SmCo rectangular pads.

Separation distances [μm]	Volume of SmCo needed to overcome gravity [μm^3]	Number of 5x10x0.25μm SmCo rectangular pads
0.5	100	8
1.0	219	18
1.5	431	35

Impact of Gold Bonding Layers

Lastly, the gold layers, in between the device and the substrate, is simulated to verify they have no effect on the force behaviors predicted above. These gold layers imitate solder or contact layers the device may have. These layers would not only restrict the minimum separation distances between device and substrate, but they

also might impact the behavior of the attractive forces. Solder layers over the SmCo were simulated using gold material, completely filling in the separation space as shown in Figure 2-23 on page 47.

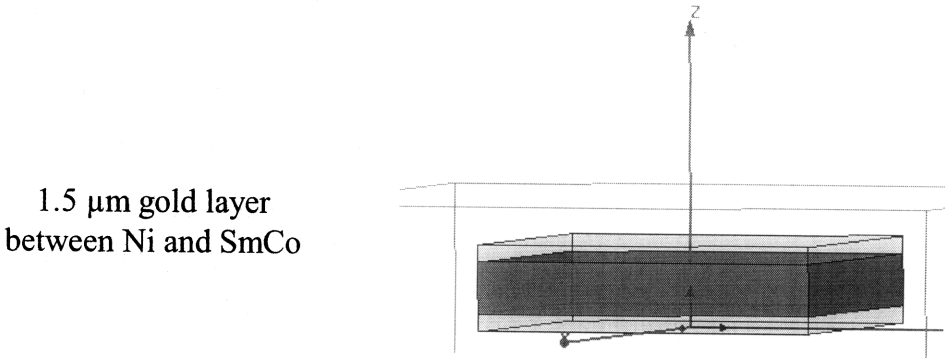

Figure 2-23: The simulation setup testing the impact of metal contact layers in between device and SmCo material. Thick layer of gold entirely fills the separation distance.

The results of the simulation are shown in table 2.2 below. There is no apparent differences in the attractive force measurements with the added gold layers. Solder layers such as gold and tin between the magnetic layers will be transparent to the magnetic fields. Thus there is no restriction on the composition of the device contact layers.

Table 2.2: Table showing attractive force measurement between the nickel plate and the SmCo magnetic material.

	Attractive force [Nt]
Without Au	3.53 E-8
With Au	3.54 E-8

2.2.6 SmCo Pattern Results based on Simulations

Based on all of the results simulated above, the following SmCo patterns were chosen, a solid 50x100μm block of magnetic material at the bottom of the recesses, a grid of thirty 5x10μm rectangles of SmCo material at the bottom of the recess, a parameter of

eighteen 5x10μm rectangles and a pattern of four 10x10μm rectangles in each corner. These can be seen in Figure 4-3 on page 69.

Since the level of device suspension depends on the mass of the device, the amount of debris and properties of the solution, different patterns corresponding to different amounts of magnetic material, were tested. Based on the calculations seen in table 2.1 above, a pattern of 18 rectangles around the perimeter of the 50x100μm rectangular recess was tested. Due to spacing issues and symmetry, a pattern of 30 filled the body of the recess floor. This pattern with 30 rectangles is less than the optimal 35 found in Table 2.1. This corresponds to a suspension distance a little less then the 1.5μm calculated. As the simulations previously described indicate, spaces between the small SmCo rectangles have minimal effect. However, to avoid problems such as a device bridging over two magnetic pads like that in Figure 2-24, spaces between recesses were designed to be greater than 100μm.

The solid block of magnetic material, referred to as Pattern 1, is the maximum amount of magnetic material seen by the device. Thus as a constant, Pattern 1 is used as a comparison. Lastly, the pattern with 4 10x10μm SmCo squares in each corner was chosen as a symmetric way of incorporating 100μm^3 of magnetic material as in Table 2.1. Thus all levels of suspension are covered based on the amount of magnetic material at the bottom of the recesses.

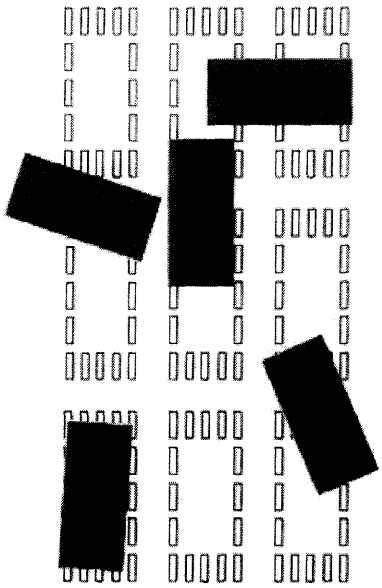

Figure 2-24: An anticipated problem where a device 50x100μm dimensions bridges between two magnetic areas.

THIS PAGE INTENTIONALLY LEFT BLANK

Chapter 3

Development of Si and III-V Materials

There are fundamental difficulties inherent in the heterogeneous integration of Si and III-V materials. These difficulties include different crystal lattice structures, different thermal expansion coefficients, and different wafer diameters. To show that Magnetically Assisted Stastical Assembly (MASA) will provide a suitable solution to these three problems, III-V heterostructure pills were used in this study. These III-V pills were then integrated into recesses on silicon substrates. Applications for this specific pair, a III-V device bonded onto a silicon substrate, include optical interconnects, fiber transceivers, and sensors. However, the MASA solution can also be used to integrate many other materials. [6]

The experimental demonstration of MASA involves fabricating a generic device to assemble, a substrate to assemble onto, magnetic material to lay on the substrate and pattern, and recess material to build on top of the magnetic material. The development of each of these parts is discussed below.

3.1 Opto Pill Development

Devices for the experiments are modeled after III-V edge emitting lasers (EEL). Typically EEL's are grown on a n-type Indium phosphide (InP) substrate along with an

InGaAs n-contact layer [8]. Prototype OptoPills were fabricated for experimentation from such an EEL heterostructure.

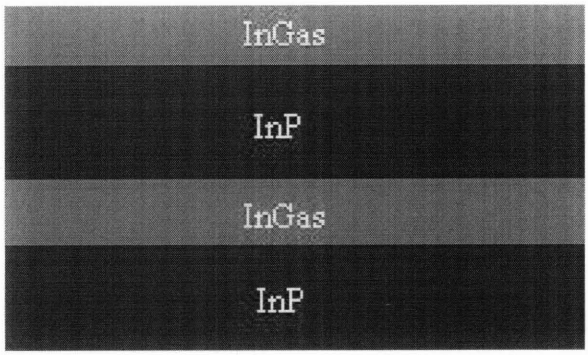

Figure 3-1: The heterostructure used to fabricate prototype OptoPills. The structure is similar to that of an EEL, but without any active lasers or mirror facets. Thickness and details in Table 3.1

OptoPills are dummy EELs made from a similar InGaAs/In heterostructure, but they do not have the ability to lase like a fully developed EEL. OptoPills have the same bulk materials but none of the mirror and active layers as seen in Figure 3-1. The contact layers are made of gold, germanium and nickel, which is layered onto the OptoPills shown in Figure 3-1. In the experiments, prototype OptoPills will represent the real device in commercial assembly.

3.1.1 Material Substrate

The structure of the optopill, grown by Professor Yoon Fatt Soon's group at Nanyang Technological University in Singapore, is a heterostructure consisting of Indium Phosphide(InP) and InGaAs layers. Table 3.1 gives the exact structure with dimensions and doping levels.

A process was developed to generate the rectangular prototype pills from this heterostructure material. An overview of the steps is as follows: 1. photo lithography for liftoff (a,b), 2. electron beam deposition of contact and soft material layers (c), 3. Reactive Ion Etch (RIE) III-V to define pills (e-f) 4. embed front surface and release substrate (g-i) 5. deposition and pattern backside contacts (j-m) [1]. 6. release

[1]All SiO_2 dry etching was done by Joseph Rumpler at Lincoln Labs.

Table 3.1: Basic OptoPill Heterostructure M1045

Layer	Thick. (nm)	Description	Material	Doping
3	200 nm	Contact Layer	In(0.53)GaAs	n+,2 E18 cm-3
2	5 μm	N-type Pill bulk	InP(n type)	n, 1-5 E17 cm-3
1	500 nm	Etch Stop Layer	In(0.53)GaAs	n+, 2 E18 cm-3
0	350 μm	(100) Substrate	InP(n type)	-

and collect optoPills (n). A general overview of the pill making process is outlined in Figure 3-2; more details may be found in Appendix A.

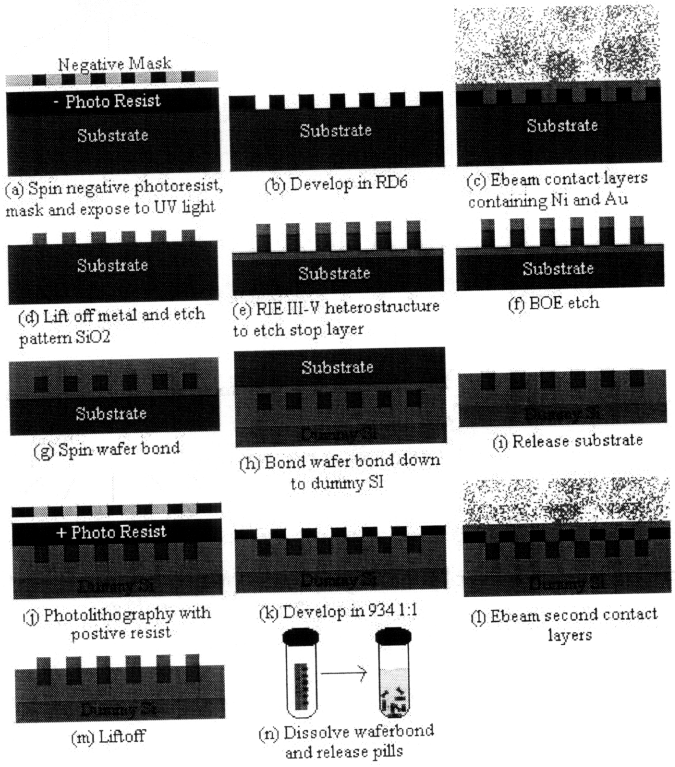

Figure 3-2: A side view of the Pill fabrication process. Details may be found in Appendix A

A micrograph of a set of processed pills ready for release and collection is shown in Figure 3-3. These devices are double side contact rectangular 50x100μm pills embedded in wafer bond. The details of this process, initially developed by Joseph Rumpler, can be found in Appendix A.

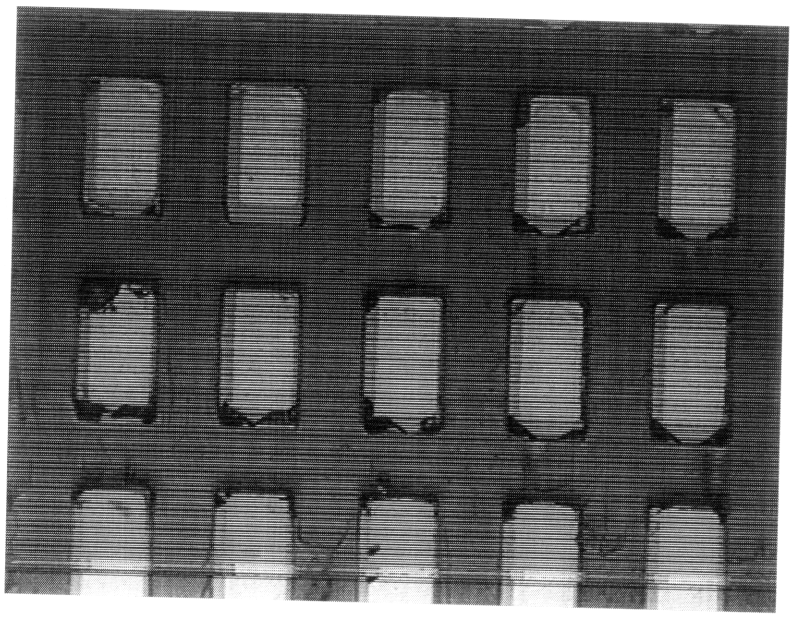

Figure 3-3: Dummy rectangular OptoPills, embedded in waferbond material. Step h in the process flow shown in Figure 3-2.

3.1.2 Contact Layers

The profile of the contact layers is listed in Table 3.2. The fifth layer is the primary soft magnetic layer in the device. The first four layers form an ohmic contact to the III-IV semiconductor, and the top gold layer provides a surface to which solder will readily adhere to permanently secure the assembled pills in the recesses. This profile has been tested and shown to create a consistent electrical contact with the device [1]. Eventually, contact layers will be placed on both faces of each device. This will increase the probability of a device floating over a recess with enough magnetic attraction.

Table 3.2: Contact Layer Profile

Layer	Material	Thickness ($\mathring{A}$)
1	Nickel	50
2	Gold	100
3	Germanium	450
4	Gold	900
5	Nickel	2500
6	Gold	2500

The thin Ni layer, Layer 1, is primarily a contact layer and although it helps in terms of magnetic attraction, Layer 5 is the primary magnetic layer. As it was seen earlier in the simulations, the amount of Ni in the device structure did not have a major bearing on the attractive force behaviors. There only needs to be a sufficient amount of nickel in the contact layers in order for the device to suspend close to the hard magnetic layer. Nickel thicknesses of 300nms was experimentally shown to be sufficient.

3.2 SmCo Hard Magnetic Material

The ferromagnetic thin film, in this case SmCo, has been previously developed in Queens collage under Professor Fred Cadieu. These in-plane magnetized Sm-Co films are synthesized with 16-18 MGOe energy products. Researchers in his lab investigate controlling the film texture of the SmCo by controlling the surface atom mobility. The magnetic material is created using pulsed laser deposition, PLD, to grow high coercivity SmCo based films. Room temperature coercivities up to 11.3 kOe have been achieved for PLD deposited films [9]. Magnetization loops for typical films used in experimentation can be found in Figure 3-9 on page 61.

3.2.1 Magnetic Film Composition

The hard magnetic patterns used for most of the experimental assembly results presented in this thesis were fabricated from Samples TD117 and TD115. Both samples were sputtered onto Cu precoated Si (100) p-type substrates. TD115 was sputtered with intrinsic coercivity of 4.4kOe, made at pressures of 100 mTorr Ar. TD117 was sputtered with intrinsic coercivity of 5.6kOe, made at pressures of 125 mTorr Ar. Both had a 30 minute Cu precoat in a separate DC magnetron sputtering system and then a 2 hour RF sputtering at 400W TDK type SmCo. The Cu layer was said to be thicker than necessary however the adhesion was satisfactory[10].

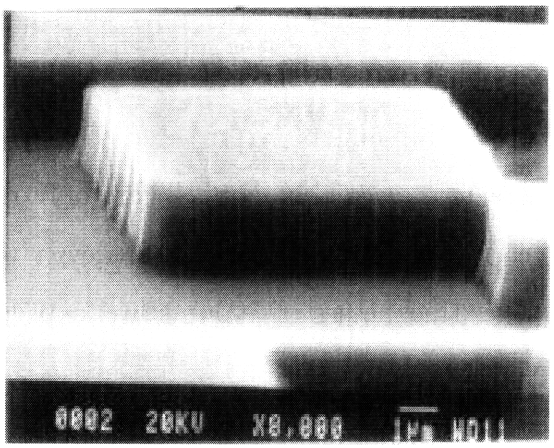

Figure 3-4: SEM micrograph of features etched into SmCo based film using a Cl_2/Ar plasma. The SiO_2 mask has been removed.

3.2.2 Patterning SmCo

Patterning the magnetic material involves a wet etch. As the magnetic material is made of SmCo, initially it was hypothesized that HCl, HNO_3, and sulfuric acid would all be able to etch the pattern. However as a photo-resist mask was used to pattern the surface, the sulfuric acid attacks the mask leaving a completely etched sample. After some experimentation, a dilute solution of HNO_3 was found to work reproducibly. A recipe of 15mL HNO_3 in 500mL of H_2O was used etching for 9 seconds. A visual indicator showed when the SmCo etching was complete as the copper below would react to the water to form copper silicide, a very rough surface resulting in a black film. In Figure 3-5, the SmCo magnetic rectangles have a color contrast to the surrounding copper silicide.

Major problems seen from this process involves undercutting the magnetic material. As the solution has a fast etching rate, an extra second would completely remove the SmCo beneath the photo-resist mask. When a sample was over etched, the sample became entirely made of copper silicide. Since feature sizes were on orders of microns, this mistake was easily made. Further problems resulted from not completely developing the photo-resist. If a sample was etched with only partially developed photo-resist, the sample resulted in pealing of the SmCo material, destroying the sample. Key points of this process were to completely develop the photo-resist as

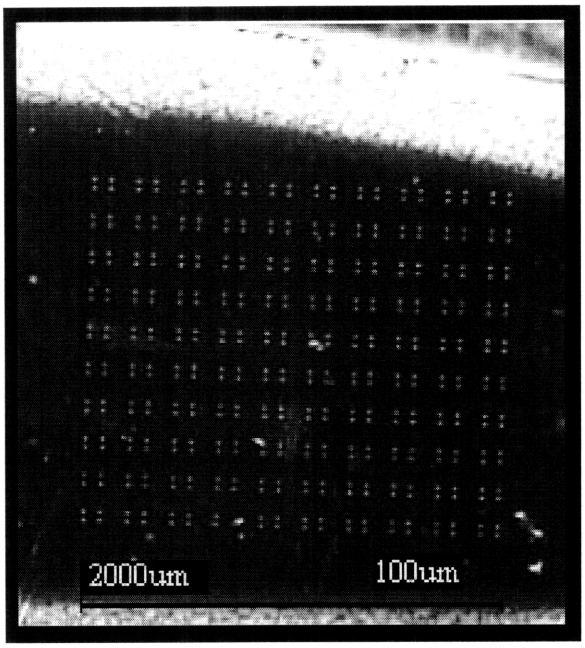

Figure 3-5: Etched magnetic pattern where light colored dots are SmCo magnetic material and darker surroundings are copper silicide.

well as be very accurate in timing the wet etch.

Also seen in Figure 3-5, a rim of lighter color appears on the edge of the sample. This is due to the properties of spinning photo-resist on a sample. The edge tends to build a thicker layer due to centrifugal forces and thus does not completely develop. This results in a thick layer of magnetic material surrounding the sample causing devices to get stuck when entering the sample. Therefore before experimentation, the portion of the substrate with this thick rim of SmCo material must be cleaved off.

3.3 Building Recesses

Once the hard magnetic material is patterned, recesses were built on top of the patterned SmCo. Several options were considered for building these recesses. Sputtering oxide, negative photo-resist, and polymers are all possibilities for building the recesses.

Past research has shown success using dielectric silicon dioxide as the bulk material for making recesses. This process involved flowing silane (SiH_4) and nitrous oxide (N_2O) into a plasma enhanced chemical vapor deposition chamber (PECVD). The

use of nitrogen helped avoid powder contaminations. This process seemed to be successful but required a lot of steps which equated to processing time and money. Also it was difficult to do perfectly and consistently as the etching time of the SiO_2 seemed to vary.

Thus, for this research, recesses were first tested using cured negative photo-resist. However a major problem was encountered during the assembly process when the Isopropanol solution, used to suspend the devices, dissolved the resist. This caused the surface to become sticky, therefore inhibiting the devices from flowing readily. This would occur within the first two minutes of assembly, regardless how long the resist was cured.

Because of the sticky nature of photo-resist, polymers were suggested. Su-8, developed by MicroChem, is a chemically amplified, epoxy based negative resist. This formula is very sensitive to near UV radiation and can be cured to be resistant against solvents, acids and bases. Once cured, it has excellent thermal stability making it near permanent in applications. Su-8 has uniform development resulting in near vertical walls. The optical transparency of the polymer also helps when aligning above magnetic patterns as seen in Figure 3-6. These properties make SU-8 ideal for recess building.

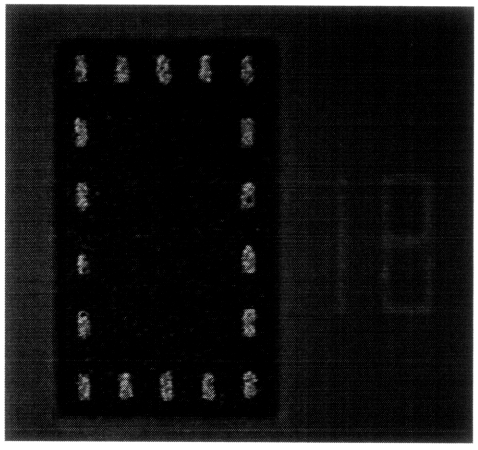

Figure 3-6: A recess in 5μm thick Su-8 aligned over eighteen 5x10μm rectangles of SmCo magnetic material. Recess dimensions are 50x100um and 5um thick.

SU-8 2005 was chosen as 5μm thick recesses were desired given the simulations above. 5μm is larger than the simulated minimum separation distance and therefore

no devices would be expected to retain unless within a recesses. Figure 3-7 is a portion of a 10 by 10 grid of recesses where each recesses is 10μm apart. This sparse grid of recesses is only for experimental purposes, as device fabrication was limited. However in actual application, recess grids would be further separated with more in excess.

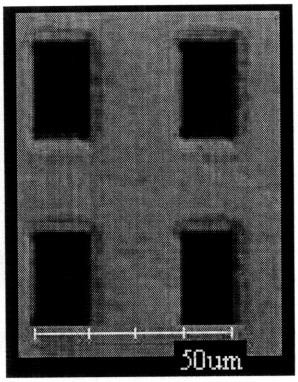

Figure 3-7: A 2x2 section of a 10x10 grid showing 5μm deep recesses each 100μm apart

3.4 ReMagnetizing the Patterned SmCo

In order to ensure that the SmCo material was magnetized, the sample was passed through an electromagnet after building the recesses. Using an electromagnet in the Fonstad lab at MIT, with a 1 cm gap, resulted in noticeably magnetized material as the sample would hang off metallic tweezers. Previously characterized by students in the Fonstad group, the I-B curve for the electromagnet is shown in Figure 3-8. At 1 cm separation gap, the electromagnet was run at maximum current of approximately 25A.

Once patterned and re magnetized, more characterizations were done to verify the sample's magnetic behavior. Below, in Figure 3-9 and Figure 3-10, are two BH curves for the TD117 and the TD115 re magnetized samples. The permanent magnet value is shown at the y axis intersection. Notice that the remanent magnetization of the TD115 is 1.21e-3EMU which is greater than the TD117 value of 1.05e-3EMU. All square device experiments were preformed on TD115 material for better comparison

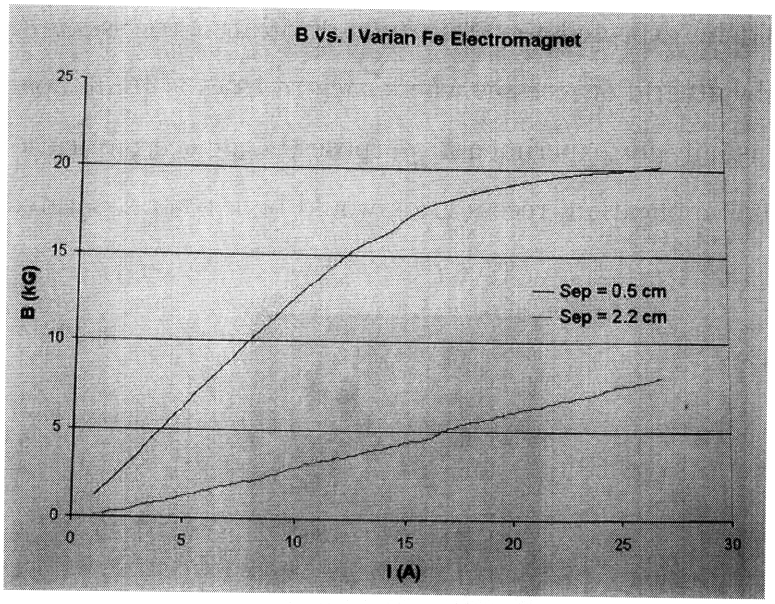

Figure 3-8: Electromagnet characterization at different gap separations.

with other square magnetic patterns. All rectangular device experiments were preformed on TD117 material. Used previously in the simulations, with Ansoft Maxwell 3D, the remanent magnetization for SmCo24 was 1.063e-3EMU. Both samples are close to this value, but material TD117 is expected to behave closer to the simulated results.

3.5 Experimental Setup

The setup for the experiments involves using a regulated pipet dripped over a beaker containing the substrate. This beaker is set on top of a tilted platform at an angle with a camera attached above to record data as seen in Figure 3-11. Major considerations were taken into account during the design, such as the angle at which the solution will flow, the rate and number of solution flowing at a given time, the container that contains the substrate, and the amount of devices flowed over the substrate at a given time. Each of these poses great difficulty to measure and will be discussed below.

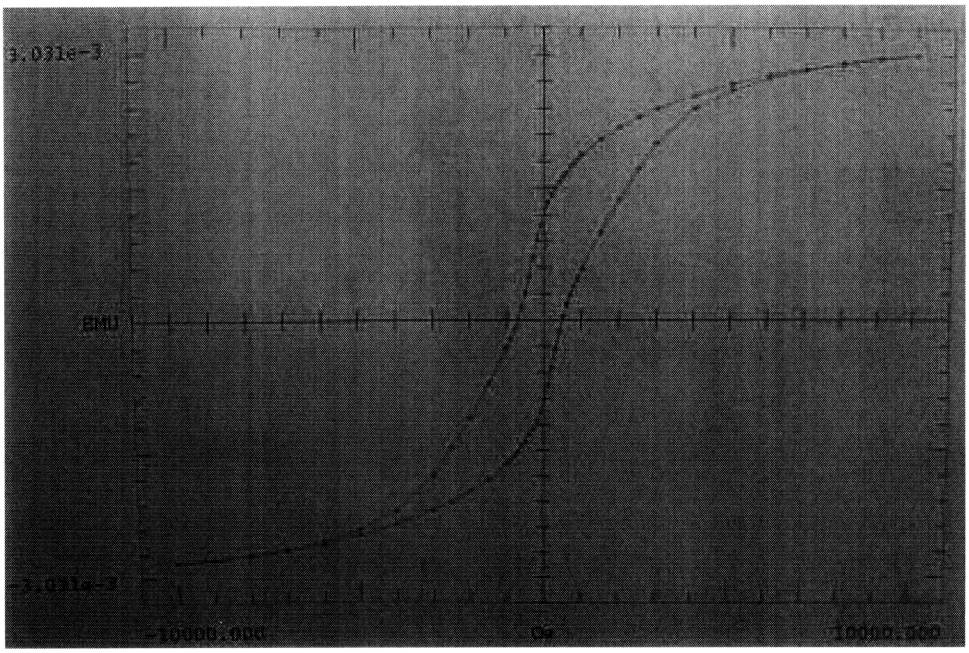

Figure 3-9: BH Digital Measurement Systems- Vibrating Sample Magnetometer for the TD115.

3.5.1 Teflon Container

A teflon, 10mL beaker was chosen as the containment unit because the pills had a tendency to stick to glass surfaces. This made using glass beakers difficult as the pills would never reach the substrate before touching glass. Teflon material was smoother and had less difficulty in getting the pills to move toward the substrate. It was found that tapping the beaker against the table would shake the pills into a neat pile near the edge of the beaker.

The size of the beaker was chosen because the substrate being filled was less than 2 mm in length and width. Therefore a small container restrained the limited number of pills to flow over instead of around the substrate; see Figure 3-11 for a picture of the beaker.

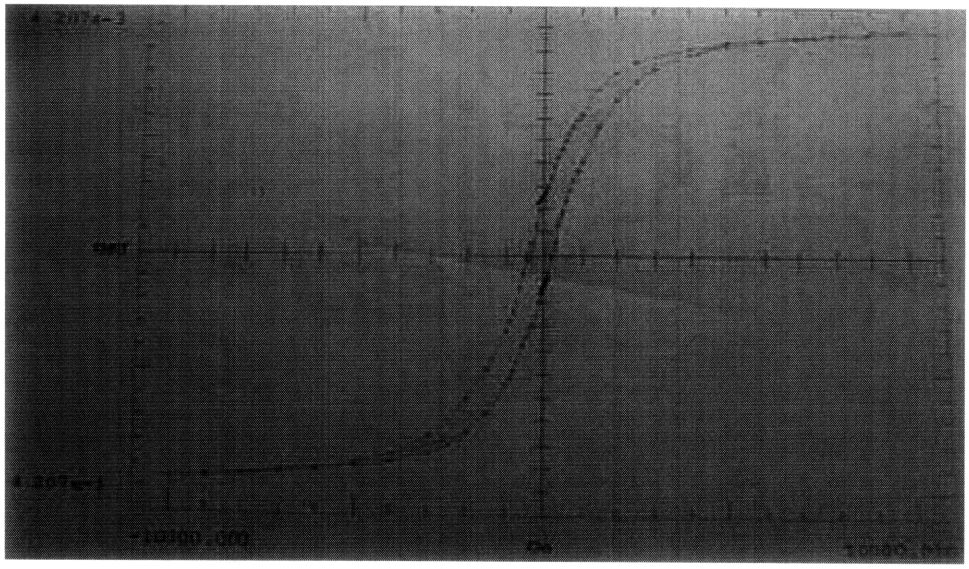

Figure 3-10: BH Digital Measurement Systems- Vibrating Sample Magnetometer for the TD117.

3.5.2 Pipet Flow Rate and Amount of Devices in Each Batch Released

The rate of the device flow is very important. If the devices flowed too fast, they would not be over the magnetic area long enough to be pulled down from suspension. If the devices flowed too slowly, they would settle to the bottom before reaching the recesses. These devices would inhibit other devices from quickly reaching the recesses and a buildup would form until the time when the devices slowly slide down the substrate, clustered in a bunch.

Thus, to limit the amount of solution released, a pipet with a small opening is used. With this pipet, the rate of release is approximately 1 drop per 3 seconds. It was found that at a certain angle, this rate of flow allowed the devices to settle low enough for magnetic attraction but at the same time not get stuck to the SU-8 polymer.

The amount of devices in each drop unfortunatly was too difficult to count. It was assumed that in total, around 300 devices would flow over the sample. This count is an estimation based on the total number of pills released into each vile. About a third of the vile was used for each sample, trying to fill 100 recesses. There were

approximately 1000 pills in each vile given from the mask pattern and the size of the heterostructure substrate used.

3.5.3 Angle of Flow

The setup in Figure 3-11 shows the beaker tilted at an angle of 20 degrees. This was experimentally determined, similar to the way flow rate was determined. A pile of OptoPills was piled at the top of the substrate, the beaker was tilted, incrementing 1 degree at a time, until the solution started to flow downwards at a reasonable rate. Visually, the pills were seen sticking near the regions with recesses. An angle of 20 degrees was used in all of the subsequent assembly studies.

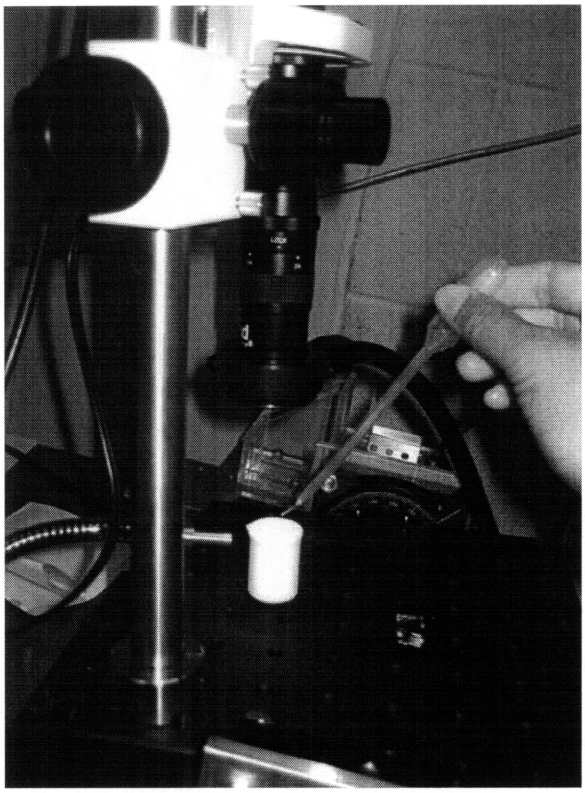

Figure 3-11: The experimental setup for filling recesses. The camera is place above a 10mL teflon beaker. The stage is rotated at an angle of 20 degrees. The pipet is inserted at the top of the substrate flowing a solution with devices over the substrate. Illumination comes from both above and on the side of the partially translucent beaker.

THIS PAGE INTENTIONALLY LEFT BLANK

Chapter 4

MASA Experimental Results

Experimental results were obtained from three main sets of experiments. The first set tested patterned SmCo samples without recesses. The second set used material TD117, with recesses, varying the different rectangular SmCo patterns. The third and last set used material TD115, with recesses, and varied the square SmCo patterns. These were designed to test simulation predictions. Each set showed behaviors that supported simulations and also gave insight to new problems.

4.1 Retentive Forces

Retention forces were tested using one sided OptoPills assembled onto patterned SmCo samples with no recesses. One sided OptoPills only have contact layers on one face of the pill, leaving the other side without soft magnetic material. With a height of 5μm thick, this should cause an upside down pill to feel insufficient attractive forces when over magnetic patterns to restrain it.

As seen in Figure 4-1, there has been evidence to show that in the worst case, without recesses to add extra separation distance, a 5μm thick separation distance is sufficient to guard against assembly of upside down pills. The magnetic 1 pattern, shown in Figure 4-3, is the maximum amount of magnetic material the device could be subjected to. As shown, a upside down device floats over a magnetic area without any indication of magnetic attraction. Therefore, regardless of the hard magnetic pattern,

the pill thickness innately restricts devices from being assembled upside down. This behavior was seen multiple times in different samples that were patterned without recesses.

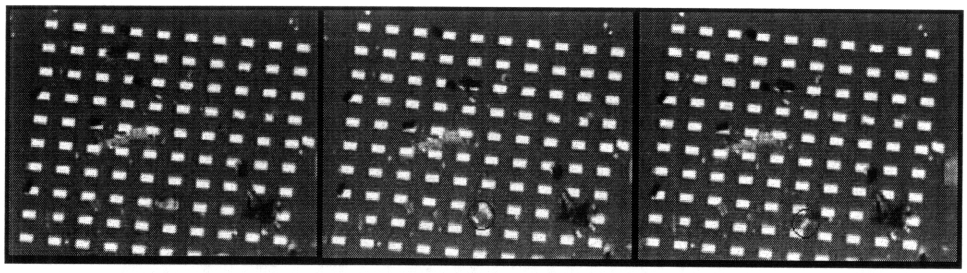

Figure 4-1: One sided pills floating over a SmCo pattern of 50x100μm rectangles (Pattern-1) with no recesses. On the left, an upside down pill floats over a magnetic pad. In the middle, the upside down pill is directly over the magnetic pad, and on the right the pill is caught in the current and floats out of place. This indicates upside down pills do not have enough retention force to hold them in place during assembly.

Retentive forces were then characterized to gain intuition on the optimal SmCo magnetic pattern. Hard magnetic patterns like those in Figure 4-3, but without recesses, and SmCo patterns like that in Figure 4-2, helped gain insight into the general characteristics of the assembly process. It can be seen that out of all the different patterns, the pattern in Figure 4-2, which only had one 5x10μm SmCo pad in each corner of the 50x100μm target area resulting in a total of four 5x10μm SmCo pads (Pattern-4), was immediately ruled out as a possible SmCo pattern. This is due the lack of retention forces from the insufficient amount of SmCo material. This follows the simulations above that indicated a minimum pattern of eighteen, 5x10μm was necessary to retain devices in the designated spot. Thus only the patterns in Figure 4-3 were tested with recesses.

4.2 Aligning Forces

Alignment was also studied without recesses on SmCo layered Si samples. Even from the beginning, without recesses, a solid Pattern-1 substrate assembled misaligned devices as seen in Figure 4-1. Without recesses, Pattern-1 would create excessive magnetic attraction to allow the pills to slide readily for alignment. Thus the solid

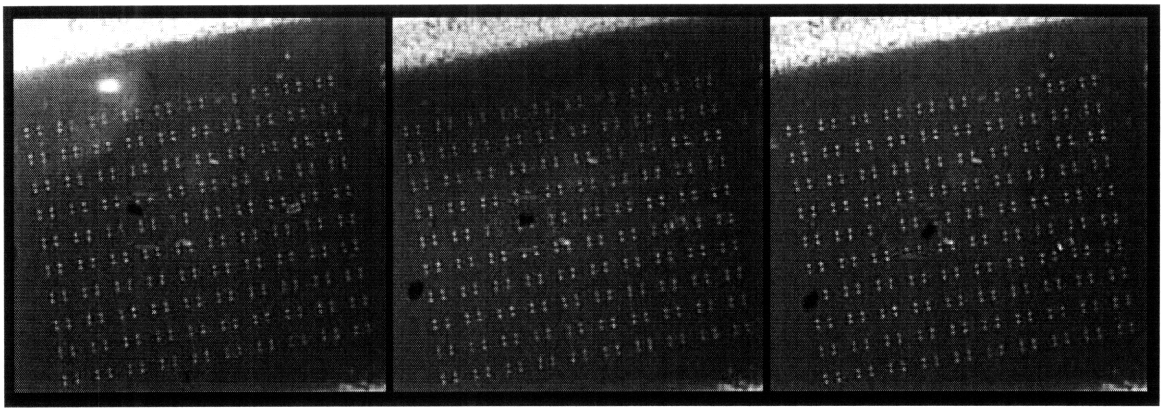

Figure 4-2: Using TD115 material and no recesses, a SmCo pattern of 4 small rectangles in each corner of a device (Pattern-4), is not enough to hold down or even attract a device from suspension. On the left, a pill is moving toward the designated assembly spot. In the middle we can see the pill is direction over the designated assembly spot and under normal circumstances should have been held down. However in the next few seconds, the device floats right over the designated spot.

Pattern-1 would have to depend on the recesses to align and orient the devices properly.

Patterns other than Pattern-1, showed indications that alignment was probable during assembly. Without recesses, each sample assembled and aligned a few devices in the target magnetic areas. However alignment was very difficult to measure as many factors could contribute. Many devices that were aligned properly seemed to be a result of the direction the solution flows. If dripped so the flow is in the same direction as the long edge of the rectangular recess, devices were more apt to assemble in the correct alignment. Other directions seemed to produce a few more devices being misaligned on samples without recesses.

4.3 Metric Definitions

To analyze and conclude results from the experimental data collected, two main metrics were used. Assembly ratio is a ratio of filled recesses versus empty recesses at the end of the 108 second experiment, representing the 24th frame of the experiment. This could mean that the maximum number of recesses filled occurs sometime before the 24th frame however the assembly ratio only takes into account the last frame at

the end of the experiment. The assembly ratio is the main metric used to determine which pattern has the best success rate and thus is the most important metric of this paper.

Shifting and or fall out rates are also metrics to help conclude which pattern has sufficient magnetic material. Shifting is used synonymously with fall out rates as they both indicate a device that has moved after being in the designated assembly target. Between each frame of the experiment, pictures of the past and the current sample are compared. Each device that was assembled in the previous picture but no longer there in the current picture, is added to the fall out rate. Thus the fall out rate is the total number of devices that have shifted out of a recess during the entire experiment.

4.4 Rectangular Recess Results

The next set of experiments add the polymer recesses above the magnetic material. Each recesses is in a grid of 10x10 recesses each separated by a minimum of 100μm for a total of 100 recesses per sample. The patterns tested are best seen in Figure 4-3. Each pattern consists of a overall rectangular shape area filled in with a SmCo magnetic pattern of smaller rectangles. These larger perimeter rectangles 50x100μm, represent target assembly pads for the devices and each 5x10μm small rectangle inside provides attractive magnetic material.

4.4.1 Rectangular Solid Pattern-1

What was observed from these sets of simulations can be seen in Figure 4-4. These pictures were taken after the standard set of 108 seconds at 1 concentrated drop of suspended devices per 3 seconds. This resulted in 24 snapshots where the pictures shown are the last of the set. As general behavior, the solid Pattern-1 demonstrated numerous misaligned devices. It took scraping and blasting large streams of solution to release the misaligned devices as they were relatively strongly held to the substrate by the solid Patterned-1 magnetic material. Having too much magnetic material led to devices partially in the recesses and partially out, devices assembled outside recesses,

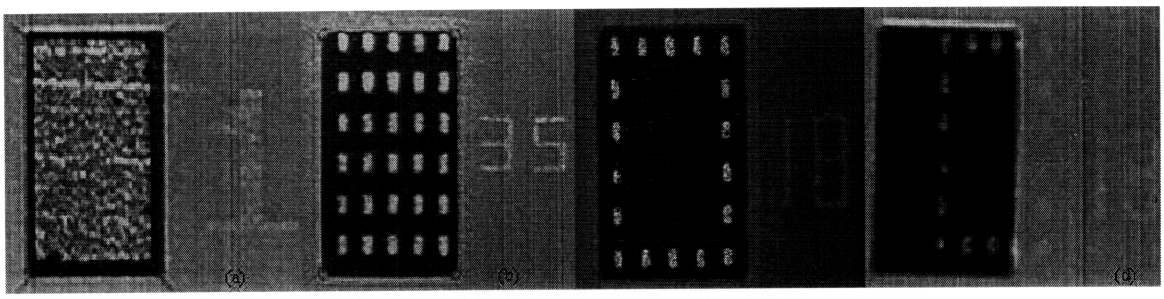

Figure 4-3: Rectangular experiments varying the SmCo, hard magnetic material, pattern at the bottom of recesses. Each sample has a grid of 10 by 10 recesses. From the left, picture (a) shows the most magnetic material tested, referred to as a solid Pattern-1, consists of a solid 50x100μm rectangular SmCo bottom layer in each recesses. Picture (b) refers to Pattern-30 for it's 30 pads of 5x10μm SmCo pads. Picture (c) shows Pattern-18, for it's 18 pads of 5x10μm SmCo pads and lastly picture (d) refers to Pattern-10, for it's 10 pads of 5x10μm SmCo pads exposed.

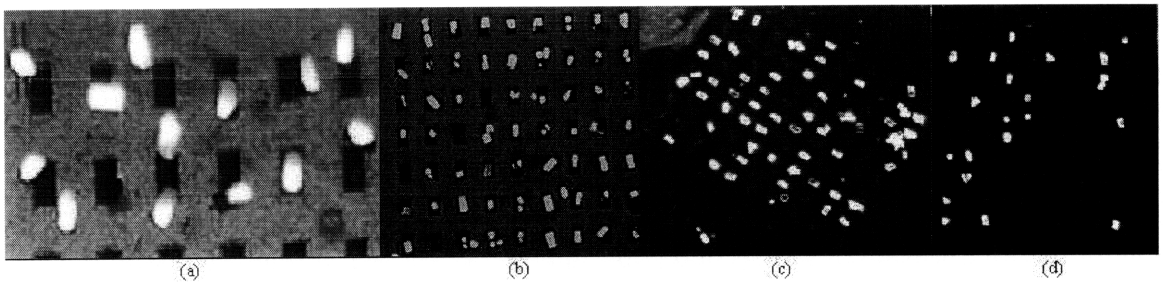

Figure 4-4: Experimental results from assembly of rectangular recesses and rectangular device pills. Picture (a) shows a solid Pattern-1, picture (b) shows a Pattern-30, picture (c) shows a Pattern-18, and picture (d) shows Pattern-10.

and recesses with two devices stacked on top of each other. This can be seen in Figure 4-5 where one device is on top of another, both being inside a recess.

To begin the analysis, results after every 3 seconds was recorded and are plotted on Figure 4-6. This figure shows the assembly trends during the experiment, ending with a assembly ratio of 22%. This ratio is determined by the number of successfully assembled devices after 108 seconds of experimentation, in the 10 by 10 grid of recesses.

With a solid Pattern-1, the behavior is dominated by the obstruction of misaligned devices permanently blocking recesses, reflected in the flatness of the plotted 24 snapshots. These obstructions to successful assembly are due to too much magnetic material. Excess SmCo leads to increased retention rates as seen in Figure 4-7,

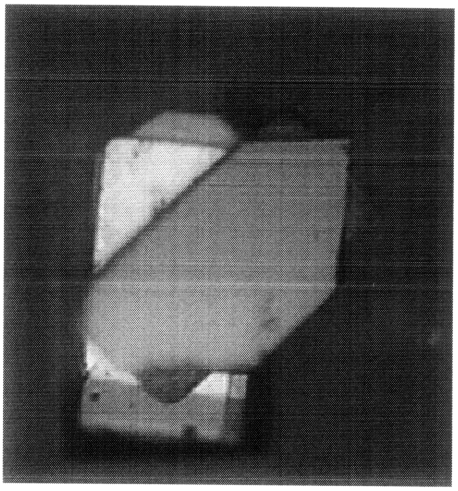

Figure 4-5: Experimental results from a solid Pattern-1. Shown is a device stacked on top of another one assembled in a recesses, indicating too much magnetic material beneath.

where each value reflects the fall out rate of a successfully assembled device over 108 seconds of experimentation. This fall out rate is determined by counting the number of devices that have shifted or 'fallen out' of a recesses every 3 seconds and adding them up for a duration of 108 second experiments. With each frame, successful device placement is recorded and if shifted or fallen out, would be counted as a fallen out device. For the Pattern-1 sample, a low average of 13 devices shifted once assembled into recesses.

4.4.2 Rectangular Pattern-10

The observations from this set of simulations can also be seen in Figure 4-4. The picture of Pattern-10 was again taken after experimentation for 108 seconds at 1 drop of concentrated devices flown over the sample for every 3 seconds. This resulted in 24 snapshots where the pictures shown are the last of the set. It was observed, as general behavior, Pattern-10 had too few devices successfully assemble. Unlike the solid Pattern-1, Pattern-10 used too little magnetic material. Thus it was observed that very few devices felt enough magnetic attraction to be pulled from suspension into the recesses.

The assembly ratio seen by Pattern-10 was 22%. However the retention of these

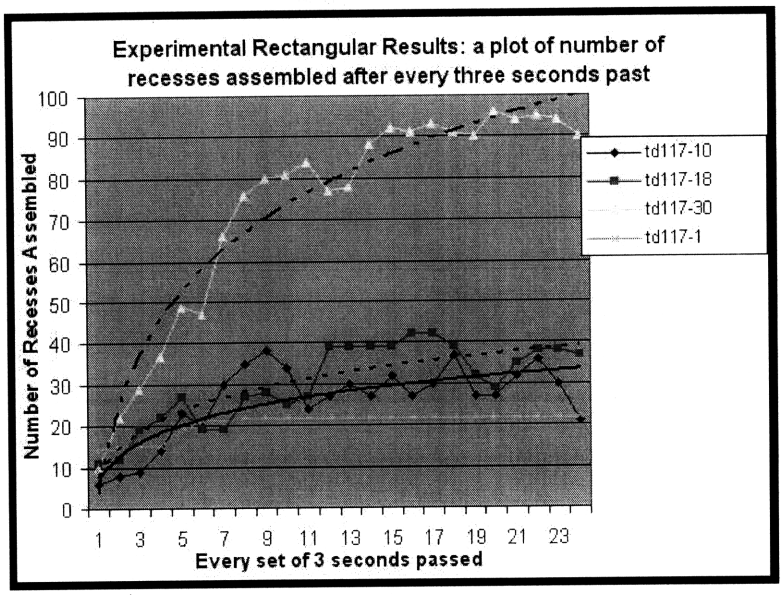

Figure 4-6: Experimental rectangular results plotting the rate of successfully filling recesses with aligned devices. Each set of data also plots logarithmic trend lines through the curves.

22 devices is very low as seen in Figure 4-7. A maximum of 32% was seen half way through the experiment however due to the low retention of the devices, these assembled devices quickly dis-assembled. This can be represented by the low curve seen in Figure 4-6, similar to the curve for the solid Pattern-1. However, unlike solid Pattern-1, the quantity of shifted devices once assembled was seen at a average of 105 during the whole experiment. 105 even exceeds the number of recesses atempting to be filled. This supports both simulation and experimental conclusions that Pattern-10 lacks sufficient hard magnetic material to retain and attract devices from the aqueous solution.

4.4.3 Rectangular Pattern-18

Pattern-18 results can also be seen in Figure 4-6 with a assembly ratio of 37%. The higher ratio correlates to a fallout occurance rate slightly lower than that of the Pattern-10. As in Figure 4-7, out of a 100 recesses experimented with 108 seconds, the fall out rate or shifting rate was observed at an average of 89. This is an improvement from the previous Pattern-10 however it is still an unacceptable rate. This decrease

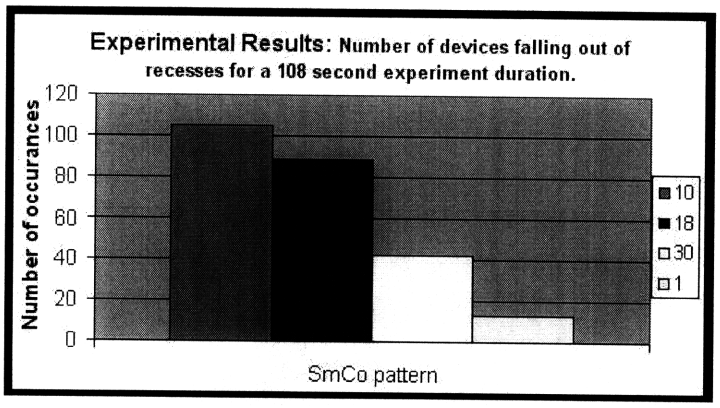

Figure 4-7: Rectangular fall out rates for the set of experiments varying hard magnetic material patterns.

in shifting rate implies that there is still not enough magnetic material at the bottom of the recess.

4.4.4 Rectangular Pattern-30

Lastly, the Pattern-30 for the rectangular experiments was tested and used [1]. Along with the best assembly ratio observed, the shifting rate is minimal as well. These results are again in Figure 4-6 where Pattern-30 curve demonstrates the largest assembly rate by far, an assembly ratio of 90%.

By the time the Pattern-30 was tested, the number of devices available for assembly was depleted to the point where most of the devices suspended were broken pieces or debris with compositions similar to the contact layers. This meant that a majority of the devices assembled were combinations of broken pieces. This could account for the high assembly ratio. Seen in Figure 4-4 recesses were often filled with two half pieces. These were counted in the assembly ratio calculations as it was assumed two small pieces would also make up a full piece. Other smaller pieces greater than half of the recess were counted as well. In the figure shown, only 4 recesses were counted as unassembled. No stacked devices were seen in this pattern like that of the solid Pattern-1 indicating that there was less excess magnetic material.

[1]Pattern-30 is labeled 35 in the fabrication mask thus a label of 35 is next to the magnetic pattern. This paper will refer to patterns by the number of small 5x10μm magnetic pads and thus 35's are referred as Pattern-30.

Because most of the devices were smaller than anticipated, the fall out rate may not correspond to commercial fall out rates. It is expected that the fall out rate be less then that of Pattern-8 but greater than that of the solid Pattern-1. This was observed however, because the devices were smaller, a lower average of fall out rate might be observed. As the device should be larger, the amount of retention felt by the device would decrease and thus would have a higher probability to shift once assembled. Then again, depending on the size of the device, more space is seen in the recesses and thus fluidic properties and SmCo pattern could increase the shifting probabilities. Therefore the fall out rate for the Pattern-30 would need to be investigated with a larger, more numerous batch of devices.

4.5 Square Recess Results

Square shapes were also tested using solid Pattern-1's and a grid of Pattern-9 with nine 5x10μm. The solid Pattern-1 was chosen again as the control of the experiment. The Pattern-9 was chosen based on the space available in a 50x50μm recess floor. These can both be seen in Figure 4-8.

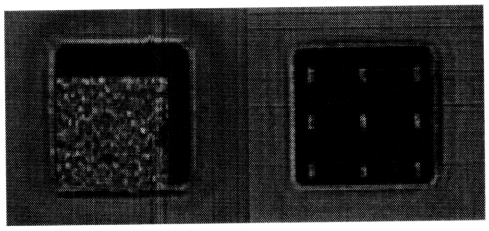

Figure 4-8: Substrate of square experiments including recess wells. On the left is the square solid Pattern-1 with a solid 50x50μm square of SmCo at the bottom of the recess. On the right is the square Pattern-9 with nine 5x10μm rectangles separated by 100μm apart.

Based on the results of rectangular analysis above, and assuming the simulations of additive squares is correct as in section 2.2.3, Pattern-15 consists of 5x10μm rectangles to provide approximately 90% assembly ratio. Therefore, Pattern-9 is expected to behave similarly to the Pattern-18 in the rectanglular experiments. The Pattern-9 in the squares show insufficient magnetic material and solid Pattern-1 is

three times too much magnetic material.

4.5.1 Square Pattern-9

Actual experimental results may be seen in Figure 4-9 below. As shown, using

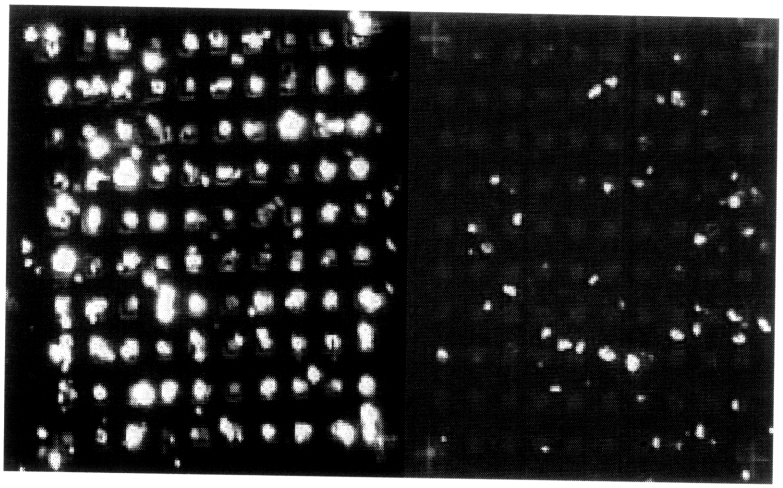

Figure 4-9: Experimental results from assembly of square recesses and square devices. On the left is the last frame for the solid Pattern-1 and on the right is the last frame for Pattern-9, both made from TD115 material.

Pattern-9 for the hard magnetic film results in low retention forces of 24% assembly ratio. The behavior of this pattern can be seen in the roughness of the curve in Figure 4-10. This up and down pattern shows little retentive forces in the recesses as if suffieicnt magnetic material was there, the curve would never dip. As expected, Pattern-9 provides insufficient hard magnetic material to retain devices inside recesses.

This idea is further enforced with Figure 4-11 showing results from a 108 second experiment demonstrating 97 devices being assembled and then shifting out of assembly. Similar to Pattern-18 rectangular experiment described above where 89 devices shifted after assembly. This high average supports the conclusion that the Pattern-9 has insufficient hard magnetic material.

As the square Pattern-9 behaves similarly to the rectangular Pattern-18, the simulation results from above are verified. Since the square is half the size of the rectangle, half the Pattern-8 is identical to the square Pattern-9. The simulation showed additive properties to the hard magnetic material as well as similar ratios of device and

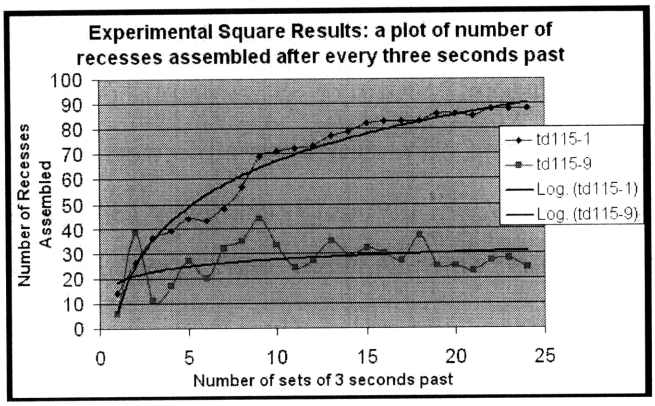

Figure 4-10: Experimental square results plotting the rate of successfully filling recesses with aligned devices. Each curve also plots logarithmic trend lines through the curves.

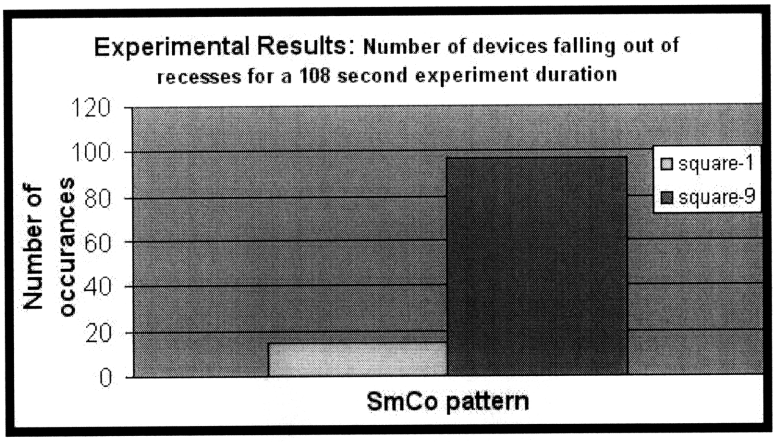

Figure 4-11: Rectangular fall out rates for the set of experiments varying hard magnetic material patterns.

SmCo geometry. These results support the simulation accuracy.

4.5.2 Square Solid Pattern-1

By the same logic as above, the square solid Pattern-1 was expected to show similar results as the rectangular solid Pattern-1. Some similarities can be seen in Figure 4-9, mainly on the left where several devices clumped together into recesses. Although it seems more than one device can fill a recess, the assembly ratio of the square Pattern-1 seems improved from the rectangular Pattern-1. It does not seem that the square devices cause obstructions to the other recesses as an assembly ratio of 88% was observed. The assembly ratio of the square Pattern-1 seems much improved from the

rectangular Pattern-1. It does not seem that the square devices cause obstructions to the other recesses as an assembly ratio of 88% was observed.

By analogy, it seems the square Pattern-1 resembles rectangular Pattern-30 more closely as they both increase drastically and break away from the other experiments in Figure 4-10 and Figure 4-6. This behavior could be explained by the misalignment of the recesses on the substrate causing less then expected magnetic material to be exposed to the device. This decrease in magnetic material could explain the increased assembly ratio.

Another explanation could come from the geometry itself. As the square devices have less alignment and orientation constraints, the probability of assembly would be expected to increase. As seen in Figure 4-12, squares have more possible assembly positions than rectangles. Increasing symmetry of the device could cause an increase in the assembly ratio.

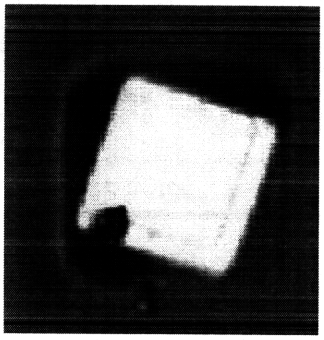

Figure 4-12: An angled square device assembled into a recess for a solid square Pattern-1.

Chapter 5

Future Work

The field of MASA technology has seen great progress over the years in experimental results from engineering SmCo hard magnetic film patterns. Simulations of magnetic behavior, magnetic layer deposition, magnetic layer patterning, and assembly of heterostructure OptoPills into recess have been successfully completed. Magnetic Pattern-30 has been successfully investigated as an excellent hard magnetic SmCo pattern for rectangular shapes and magnetic pattern a little less than Pattern-1 has been concluded as a good hard magnetic SmCo pattern for square shapes. For future continuation in developing MASA technology, patterning the soft magnetic material on the device side must be investigated. This could further ensure perfect alignment within the recess. As it was seen in the experiments, the devices would be generally aligned within a recess but depending on the exact size of the recess and device, there was leeway for slight misalignments. This could be alleviated by engineering a complementary soft magnetic geometry to fit into the hard magnetic pattern at the bottom of the recesses in a lock and key manner, demonstrated in Figure 5-1.

Further investigation could be done to characterize the effects of increasing and decreasing the amount of magnetic material. Ideally, as Pattern-30 gave a 90% fill ratio, a sample with slightly more SmCo should be experimented with to increase the fill ratio. Incrementally adding more 5x10μm squares to the bottom of the recess could provide a more accurate characterization of the retentive forces. A higher fill ratio may be achieved with increasing magnetic material above Pattern-30 but below

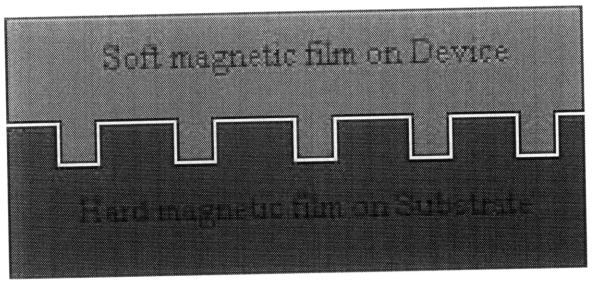

Figure 5-1: A demonstration of the advantages to patterning soft magnetic material as a complementary fit to the hard magnetic material at the bottom of the recess.

solid Pattern-1.

A suggestion for future experiments includes larger quantities of quality devices to increase fill ratios of complete devices instead of several broken pieces of debris metal. In order to purify the solution of devices, centrifuging is a possibility. With larger quantities of devices, a larger gradient can separate out partially broken devices from fully fabricated devices. The exact spin setting would need to be characterized based on the weight of the device. Also to purify the solution of devices, single sided contact devices should be used instead of double sided. In the last steps of device fabrication, depositing the second face with contact layers causes large amounts of debris containing Ni layers. This debris was often seen obstructing device assembly by filling in the recess or clumping with the device making devices too big to fit into the recess.

Also for device improvements, different shape characterizations should be performed in order to fully understand the geometric factor in the assembly ratio. As seen with the square device, different probabilities of assembly occur. A circular device may further increase the assembly ratio as any orientation faced up is acceptable. This many cause some of the inconsistencies in the simulations.

In terms of the setup of the experiment, improvements could be made in automating the pill releasing mechanism. Currently, a drop of OptoPills is released manually every 3 seconds of the experiment. This manual release can be inconsistent at times depending on the pipet used and thus the fill ratio may benefit from improvements on releasing devices. Furthermore, the beaker used to contain the substrate was not as

form fitting as it should be. The extra leeway in space caused difficulties in controlling the flow of the devices. A more channeled container directing solutions suspended with devices directly over the recesses, may also increase assembly rates. Also a sonic vibrator could be attached to the platform to decrease devices that obstruct other recess assembly.

For the magnetic material, different types of compositions should be tried. Copper Silicide is not an ideal material to have at the base of the substrate. A bare Si composition, and a Tantalum (Ta) composition could provide better results without a Cu bi-product. The wet etch recipe would need characterization as well since the dilute HNO_3 may react with the new compounds. This would improve the commercial application of MASA technology as copper silicide potentially poses a problem in device applications.

THIS PAGE INTENTIONALLY LEFT BLANK

Appendix A

Process Recipes

A.1 OptoPill Process Recipe

The following recipes are expanded descriptions of the lithography used to create OptoPills. All recipes were initially developed by Joseph Rumpler, a fellow graduate student at MIT, who first worked on the MASA project. All masks were designed as tools to complete these processes. Steps are described in order as follows:

A.1.1 Photolithography

Spinning a photo resist mask to define shape of the OptoPill devices.

1) Solvent clean samples (Acetone, Methanol, IPA, N_2 blow dry)

2) Place on 150 degree hotplate to dry

3) Coat NR7-1000py at 3000rpm for 30 seconds

4) Hotplate at 150 degrees for 1.5 minutes

5) High resolution expose for 20-30 seconds using the high filter lense

6) Hotplate at 100 degrees for 1-2 minutes

7) Develop in RD6 for 10-30 seconds

A.1.2 Contact Layers

Electron beam deposition on contact layers

1) Electron beam deposit at pressures of 1.6E-6 mTorr.

2) Deposit Nickel at 50 ($\mathring{A}$)

3) Deposit Gold at 100 ($\mathring{A}$)

4) Deposit Germanium at 450 ($\mathring{A}$)

5) Deposit Gold at 900 ($\mathring{A}$)

6) Deposit Nickel at 2500 ($\mathring{A}$)

7) Deposit Gold at 2500 ($\mathring{A}$)

8) Liftoff in acetone

A.1.3 Pill Wafer bonding

After SiO_2 dry etching,

1) BOE dip for 7.5 minutes

2) Spin wafer bond, 2000rpm 20 seconds

3) Heat 110 degrees C, 1.5 minutes

A.1.4 Bonder

Using the pill bonder developed by Mindy Teo at the Fonstad lab at MIT, the pills are then bonded to a piece of silicon.

1) Place a glass cover slide on the black ceramic.

2) Put the silicon piece facing up, on the slide. Place the pills face down on the silicon piece.

3) Cover with aluminum foil. Tighten screws.

4) Rough pump, Nitrogen, Forming gas flow each 5 minutes.

5) Program and run:

Program number	Temperature (°C)	Duration (min)
1	100	1
2	160	6
3	10	end

A.1.5 Second Side Contact Layer

1) Etch HCL until bubbles are eliminated. approximately 1.21hours, etch rate 6μ/min.

2) NR7-3000p static dispense 3000rpm, 35 seconds

3) Hotplate 100 degC bake 2 minutes

4) Expose high resolution alignment 45-52seconds, align using smaller pattern

5) Hotplate 100 degC bake 3 minutes

6) Develop RD-6 60 seconds

7) BOE dip 5 seconds

8) Ebeam second contact layer as before

A.1.6 Indian Phosphide Etch

To remove the etch stop layer from the backside.

1) Make solution 1:1:20 Sulfuric acid:hydrogen peroxide: H_2O. approximately 20mL:20mL:400mL

2) Etch 1.5 minutes

A.1.7 Release Pills

To release, clean and store pills in glass vile.

1) Fill vile with wafer bond remover

2) Place sample in and swirl

3) Siphon out wafer bond, take care not to siphon out pills

4) Rinse with acetone (repeat twice)

5) Rinse with methanol

6) Rinse with isoproponal (repeat three times)

7) Store viles in moderate temperatures

A.2 Etching SmCo Magnetic Material

Using positive resist to mask the pattern, then using a wet etch to remove the SmCo down to the copper layer.

A.2.1 Photolithography

Spinning a photo resist mask to define the magnetic pattern. Do not use HMDS as it will cause complications in dissolving the OCG positive resist.

1) Solvent clean samples (Acetone, Methanol, IPA, N_2 blow dry)

2) OCG-825 static dispense, 3k rpm, 35 seconds total

3) Oven bake 90 degrees C, 30 minutes

4) Expose .55min High Res Aligner

5) Develop in 934 1:1 for 55 seconds

A.2.2 Wet Etch Dilute HNO_3

This process is very time sensitive. One extra second can cause over etching by 20μm. Will often undercut the photo-resist.

1) Solvent clean samples (Acetone, Methanol, IPA, N_2 blow dry)

2) 15:500 parts H_2O:HNO_3 in glass beaker

3) Stir for 20 seconds

4) Dip sample for 9 seconds until turns black, 100nm etch/6seconds

A.3 SU-8 Recess Building

Building polymer recesses over etched SmCo magnetic patterns.

1) Pre-bake samples on hotplate 95^o

2) SU-8 2005 static dispense 3000rpm, 30 seconds

3) Hotplate 95^o, 2 minutes

4) Align larger pattern on low res aligner and expose for 45 seconds

5) Post expose Hotplate 95^o, 3 minutes

6) Develop pm Acetate 30 seconds

THIS PAGE INTENTIONALLY LEFT BLANK

Bibliography

[1] Joseph John Rumpler, "Optoelectronic Integration Using the Magnetically Assisted Statistical Assembly Technique: Initial Magnetic Characterization and Process Development," Masters thesis, Massachusetts Institute of Technology, September 2002.

[2] Mindy Simin Teo, "Development of Pick-and-Place Assembly Techniques for Monolithic Optopill Integration ," Masters thesis, Massachusetts Institute of Technology, February 2005

[3] Sudhakar Shet, Vishal R. Mehta, Anthony T. Fiory, "The Magnetic Field-Assisted Assembly of Nanoscaled Semiconductor Devices: A New Technique," *JOM: Silicon Nanoelectronics*, pp. 32-34, October 2004

[4] Ikuo Soga, Yutaka Ohno, Shigeru Kishimoto, "Fluidic Assembly of Thin GaAs Blocks on Si Substrates," *The Japan Society of Applied Physics*, Vol. 42, pp. 2226-2229, Part 1, No 4B, April 2003

[5] Joseph John Rumpler, "Assembly and Magnetic Retention of Hetergeneous Materials and Devices," *RQE*, September 2005

[6] Clifton G. Fonstad, Fed Cadieu, "Collaborative Research: Magnetically Assisted Stochastic Assembly," *National Science Foundation*, October 2006

[7] J. S. Gustavsson, *IEEE J. Quant. Electr.*, Vol. 38, pp. 203-214, 2002

[8] Y. Ohiso, "Single Transverse mode operation of 1.55 m buried heterostructure vertical-cavity surface emitting lasers," *IEEE Phot. Tech. Lett.*, Vol. 14, pp.738-40, 2002

[9] F.J.Cadieu, "Systematics of Permanent Magnetic Film Texturing and the Limits of Film Synthesized 1-12 and 2-17 Iron Based Rare Earth Transition Metal Permanent Magnet Systems," New York:Queens Collage, January 1998

[10] F.J.Cadieu, private communication